

Additive Density-on-Scalar Regression in Bayes Hilbert Spaces with an Application to Gender Economics

Eva-Maria Maier¹, Almond Stöcker¹, Bernd Fitzenberger², and Sonja Greven¹

¹*Chair of Statistics, School of Business and Economics, Humboldt-Universität zu Berlin, Germany*

²*IAB (Institute for Employment Research), Nuremberg, Germany*

Abstract

Motivated by research on gender identity norms and the distribution of the woman's share in a couple's total labor income, we consider functional additive regression models for probability density functions as responses with scalar covariates. To preserve nonnegativity and integration to one under summation and scalar multiplication, we formulate the model for densities in a Bayes Hilbert space with respect to an arbitrary finite measure. This enables us to not only consider continuous densities, but also, e.g., discrete or mixed densities. Mixed densities occur in our application, as the woman's income share is a continuous variable having discrete point masses at zero and one for single-earner couples. We discuss interpretation of effect functions in our model via odds-ratios. Estimation is based on a gradient boosting algorithm, allowing for potentially numerous flexible covariate effects. We show how to handle the challenging estimation for mixed densities within our framework using an orthogonal decomposition. Applying this approach to data from the German Socio-Economic Panel Study (SOEP) shows a more symmetric distribution in East German than in West German couples after reunification and a smaller child penalty comparing couples with and without minor children. These West-East differences become smaller, but are persistent over time.

Keywords: Density Regression; Functional Additive Model; Gradient Boosting; Mixed Densities.

1 Introduction

Analyzing the distribution of the female income share for couples in the U.S., Bertrand et al. (2015) show that the fraction of couples with a share below 0.5 is much higher than the fraction of those with a share above 0.5 and that there is

a discontinuous drop in the density at 0.5. This drop is attributed to gender identity norms with men being averse to a situation with their female partners making more money than themselves. Subsequent studies, however, showed mixed results (e.g., Sprengholz et al., 2020; Kuehnle et al., 2021). Most of the literature does not consider how the share distribution changes depending on covariates, but this in itself is of great interest. Social norms change over time towards higher employment of females, with part-time employment becoming more prevalent, especially in the presence of children. And the employment and earnings of female partners show a strong childhood penalty (Kleven et al., 2019; Fitzenberger et al., 2013).

From a methodological perspective, the focus on a univariate analysis of the share distribution reflects the lack of an interpretable multivariate analysis of its determinants. Filling this gap, we introduce a regression approach for outcomes that are probability density functions with scalar covariates and we use this new approach to analyze how the female income share distribution in Germany varies by place of residence (e.g., between West and East Germany), the presence of children, and over time.

For the continuous density case, our approach could be viewed as a special case of functional regression, which is part of the vast field of functional data analysis (e.g., Ramsay and Silverman, 2005). One usually distinguishes three types of functional regression models (e.g., Brockhaus et al., 2015): *scalar-on-function*, where the response is scalar while the covariates are functions, *function-on-scalar* with functional response and scalar covariates and *function-on-function*, where both, response and covariates, are functions. Analogously, we refer to our regression setting as *density-on-scalar*. Existing function-on-scalar methods are not applicable in this case, as multiplying a density with a negative scalar or adding two densities in the classical sense immediately violates the nonnegativity and integrate-to-one constraints of densities. An appropriate alternative normed vector space structure for densities is provided by Bayes Hilbert spaces, motivated by Aitchison’s work about compositional data (Aitchison, 1986). Egozcue et al. (2006) first introduced Bayes Hilbert spaces for densities with respect to the Lebesgue measure on a finite interval. This was extended by Boogaart et al. (2014) to Bayes Hilbert spaces on finite measure spaces. Talská et al. (2018) use Bayes Hilbert spaces for linear density-on-scalar regression, considering only densities defined on a finite interval and Lebesgue integrals. For estimation, the model is mapped into a subspace of the L^2 of square integrable functions applying the centered log-ratio (clr) transformation. We extend their framework to additive density-on-scalar regression models for densities on arbitrary finite measure spaces. This enables us to handle not only densities with respect to the Lebesgue measure on a finite interval (*continuous case*) or to the weighted sum of Dirac measures on a finite set (*discrete case*) but also mixtures of both (*mixed case*) in a unified framework. We introduce a gradient boosting algorithm based on the approach of Hothorn et al. (2014), enabling estimation directly in the Bayes Hilbert space. Furthermore, we develop a method to interpret the estimated effects analogously to odds ratios. In our motivating application, we analyze the distribution of the woman’s share in a couple’s total labor income in Germany – an example of the mixed case: The corresponding densities defined on $[0, 1]$ have positive point mass at the boundary values 0 and 1, corresponding to single-earner

couples. This leads to a mixed (Dirac/Lebesgue) reference measure.

Apart from the Bayes Hilbert space approach, different ideas for density regression have been proposed. Park and Qian (2012) discuss density-on-density regression without any positivity constraints, performing linear regression directly on the deviations from the mean density. Petersen and Müller (2019) present linear regression for densities based on the Wasserstein metric, which constitutes a popular approach to statistical analysis of distributional data (Ollivier et al., 2014). However, with this approach the densities are considered in a nonlinear space, which makes modeling and interpretation more difficult. Han et al. (2020) introduce additive functional regression models for the density-on-scalar case as well. They transform the densities to the L^2 , in particular proposing the log hazard and the log quantile density transformations. Happ et al. (2019) show that for both, numerical instabilities may occur and finally prefer the clr transformation to both. In contrast to Han et al. (2020), which only considers the transformed densities for modeling, our Bayes Hilbert space approach provides an entire conceptual framework that allows to embed the densities and specify the model in a vector space structure. The clr transformation, an isometric isomorphism, allows an equivalent formulation in the L^2 , which enables appealing odds-ratio-type interpretations on the original density-level.

Density regression is related to several other areas of research. For the discrete case, also known as compositional data (i.e., a multivariate vector of non-negative fractions summing to one, e.g., Pawlowsky-Glahn et al., 2015), regression has also been studied, with Boogaart et al. (2015) for instance considering Bayesian regression with compositional response. In general, there are also approaches not modeling densities but equivalent functions. E.g., Yang et al. (2018) present a Bayesian approach to model quantile functions as response in a functional linear regression by introducing their quantlet basis representation. In contrast, modeling the density function has the distinct advantage that shifts of probability masses and special characteristics of the distribution such as bimodality can be identified straightforwardly. All methods mentioned so far share the assumption that a sample of densities (or, e.g., quantile functions) has been observed (or estimated). In contrast, there are also individual-level approaches, which model the conditional density or equivalent functions given covariates based on a sample of individual scalar data. Parametric approaches such as generalized additive models for location, scale and shape (GAMLSS, also known as distributional regression; e.g., Rigby and Stasinopoulos, 2005) require a known distribution family and only enable interpretation on the level of their parameters, not the distribution, which can be restrictive. In quantile regression (e.g., Koenker, 2005) no specific distribution family is assumed, but for each quantile of interest one model has to be estimated, which is potentially computationally demanding. Furthermore, the estimated quantiles may cross, which can be avoided, e.g., by monotonization or rearrangement (e.g., Chernozhukov et al., 2010). Conditional transformation models (CTMs, e.g., Hothorn et al., 2014) model a monotone transformation function, which transforms the conditional distribution function (cdf) of the response to an a priori specified reference distribution function, in terms of covariates. In distribution regression (e.g., Chernozhukov et al., 2013), the cdf is estimated pointwise, similarly as in quantile regression. It requires the choice of a link function between the conditional distribution and the parametric

covariate effects. Moreover, there are Bayesian (e.g., MacEachern, 1999), kernel estimation (e.g., Takeuchi et al., 2006), and machine learning approaches (e.g., Li et al., 2021) for modeling conditional response densities, suffering from two limitations: They work with a relatively large number of hyper-parameter(-distribution)s which influence the outcome; related to this is their lack of interpretability, in particular in terms of the covariate effects.

We aim to bridge this gap in the literature by directly modeling the response density on the one hand, while borrowing interpretable yet flexible additive models from functional data analysis on the other hand. To the best of the authors' knowledge, our approach is the first to cover continuous, discrete and mixed cases in a unified framework.

In the following, Section 2 summarizes the construction of Bayes Hilbert spaces. Section 3 introduces our density-on-scalar regression approach, where models are formulated in Bayes Hilbert spaces and estimated using a boosting algorithm. In the mixed case, we derive an orthogonal decomposition of the Bayes Hilbert space to facilitate (separate continuous/discrete) estimation. We develop an interpretation method of the estimated effects using odds-ratios. Section 4 involves a comprehensive application for the mixed case in analyzing the distribution of the woman's share in a couple's total labor income in Germany. Section 5 provides a small simulation study based on our application setting to validate our approach. We conclude with a discussion and an outlook in Section 6.

2 The Bayes Hilbert space

We briefly introduce Bayes spaces and summarize their basic vector space properties for a σ -finite reference measure as described in Boogaart et al. (2010). Refining these to Bayes Hilbert spaces (Boogaart et al., 2014), we have to restrict ourselves to finite reference measures. We provide proofs for all theorems in appendix A.1 since we take a slightly different point of view compared to Boogaart et al. (2010) and Boogaart et al. (2014).

Let $(\mathcal{T}, \mathcal{A})$ be a measurable space and μ a σ -finite measure on it, the so-called *reference measure*. Consider the set $\mathcal{M}(\mathcal{T}, \mathcal{A}, \mu)$, or short $\mathcal{M}(\mu)$, of σ -finite measures with the same null sets as μ . Such measures are mutually absolutely continuous to each other, i.e., by Radon-Nikodyms' theorem, the μ -density of ν or Radon-Nikodym derivative of ν with respect to μ , $f_\nu := d\nu/d\mu : \mathcal{T} \rightarrow \mathbb{R}$, exists for every $\nu \in \mathcal{M}(\mu)$. It is μ -almost everywhere (μ -a.e.) positive and unique. We write $f_\nu \cong \nu$ for a measure $\nu \in \mathcal{M}(\mu)$ and its corresponding μ -density f_ν . For measures $\nu_1, \nu_2 \in \mathcal{M}(\mu)$, let the equivalence relation $=_{\mathcal{B}}$ be given by $\nu_1 =_{\mathcal{B}} \nu_2$, iff there is a $c > 0$ such that $\nu_1(A) = c\nu_2(A)$ for every $A \in \mathcal{A}$, where $c(+\infty) = +\infty$. Respectively, we define $f_{\nu_1} =_{\mathcal{B}} f_{\nu_2}$, iff $f_{\nu_1} = cf_{\nu_2}$ for some $c > 0$. Here and in the following, pointwise identities have to be understood μ -a.e. Both definitions of $=_{\mathcal{B}}$ are compatible with the Radon-Nikodym identification $f_\nu \cong \nu$. The set of $(=_{\mathcal{B}})$ -equivalence classes is called the *Bayes space (with reference measure μ)*, denoted by $\mathcal{B}(\mu) = \mathcal{B}(\mathcal{T}, \mathcal{A}, \mu)$. For equivalence classes containing finite measures, we choose the respective probability measure as representative in practice. Then, the corresponding μ -density is a probability density. However, mathematically it is

more convenient to use a non-normalized representative. For better readability, we omit the index \mathcal{B} in $=_{\mathcal{B}}$ and the square brackets denoting equivalence classes in the following. For $f_{\nu_1} \cong \nu_1, f_{\nu_2} \cong \nu_2 \in \mathcal{B}(\mu)$, the addition or *perturbation* is given by the equivalent definitions

$$(\nu_1 \oplus \nu_2)(A) := \int_A \frac{d\nu_1}{d\mu} \frac{d\nu_2}{d\mu} d\mu, \quad f_{\nu_1} \oplus f_{\nu_2} := f_{\nu_1} f_{\nu_2}.$$

For $f_{\nu} \cong \nu \in \mathcal{B}(\mu)$ and $\alpha \in \mathbb{R}$, the scalar multiplication or *powering* is defined by

$$(\alpha \odot \nu)(A) := \int_A \left(\frac{d\nu}{d\mu} \right)^{\alpha} d\mu, \quad \alpha \odot f_{\nu} := (f_{\nu})^{\alpha}.$$

Theorem 2.1 (Boogaart et al., 2010). *The Bayes space $\mathcal{B}(\mu)$ with perturbation \oplus and powering \odot is a real vector space with additive neutral element $0 := \mu \cong 1$, additive inverse element $\ominus \nu := \int_A d\mu/d\nu d\mu \cong 1/f_{\nu}$ for $\nu \in \mathcal{B}(\mu)$, and multiplicative neutral element $1 \in \mathbb{R}$.*

For subtraction, we write $\nu_1 \ominus \nu_2 := \nu_1 \oplus (\ominus \nu_2)$ and $f_{\nu_1} \ominus f_{\nu_2} := f_{\nu_1} \oplus (\ominus f_{\nu_2})$. From now on, we restrict the reference measure μ to be finite, progressing to Bayes Hilbert spaces. This is similar to Boogaart et al. (2014) with some details different. In the style of the well-known L^p spaces, B^p spaces for $1 \leq p < \infty$ are defined as

$$B^p(\mu) = B^p(\mathcal{T}, \mathcal{A}, \mu) := \left\{ \nu \in \mathcal{B}(\mu) \mid \int_{\mathcal{T}} \left| \log \frac{d\nu}{d\mu} \right|^p d\mu < \infty \right\}.$$

We also say $f_{\nu} \in B^p(\mu)$ for $f_{\nu} \cong \nu \in B^p(\mu)$. This is equivalent to $\log f_{\nu} \in L^p(\mu)$, which gives us $B^q(\mu) \subset B^p(\mu)$ for $p, q \in \mathbb{R}$ with $1 \leq p < q$. Note that for every $p \in \mathbb{R}$ with $1 \leq p < \infty$, the space $B^p(\mu)$ is a vector subspace of $\mathcal{B}(\mu)$, see Boogaart et al. (2014). For $f_{\nu} \cong \nu \in B^p(\mu)$, the *centered log-ratio (clr) transformation* of ν is given by

$$\text{clr}_{B^p(\mathcal{T}, \mathcal{A}, \mu)}[\nu] = \text{clr}_{B^p(\mathcal{T}, \mathcal{A}, \mu)}[f_{\nu}] := \log f_{\nu} - \mathcal{S}_{B^p(\mathcal{T}, \mathcal{A}, \mu)}(f_{\nu}), \quad (2.1)$$

with $\mathcal{S}_{B^p(\mathcal{T}, \mathcal{A}, \mu)}(f_{\nu}) := 1/\mu(\mathcal{T}) \int_{\mathcal{T}} \log f_{\nu} d\mu$ the mean logarithmic integral. We omit the indices $B^p(\mathcal{T}, \mathcal{A}, \mu)$ or shorten them to μ or \mathcal{T} , if the underlying space is clear from context.

Proposition 2.2 (For $p = 1$ shown in Boogaart et al., 2014). *For $1 \leq p < \infty$, the clr transformation $\text{clr} : B^p(\mu) \rightarrow L_0^p(\mu) := \{\tilde{f} \in L^p(\mu) \mid \int_{\mathcal{T}} \tilde{f} d\mu = 0\}$ is an isomorphism with inverse transformation $\text{clr}^{-1}[\tilde{f}] = \exp \tilde{f}$.*

Note that $L_0^p(\mu)$ is a closed subspace of $L^p(\mu)$. The space $B^2(\mu)$ is called the *Bayes Hilbert space* (with reference measure μ). For $f_{\nu_1} \cong \nu_1, f_{\nu_2} \cong \nu_2 \in B^2(\mu)$, consider

$$\langle \nu_1, \nu_2 \rangle_{B^2(\mu)} := \langle f_{\nu_1}, f_{\nu_2} \rangle_{B^2(\mu)} := \int_{\mathcal{T}} \text{clr}[f_{\nu_1}] \text{clr}[f_{\nu_2}] d\mu,$$

which is an inner product on $B^2(\mu)$, see Proposition A.1 in appendix A.1. It induces a norm on $B^2(\mu)$ by $\|\nu\|_{B^2(\mu)} := \|f_{\nu}\|_{B^2(\mu)} := \sqrt{\langle f_{\nu}, f_{\nu} \rangle_{B^2(\mu)}}$ for $f_{\nu} \cong \nu \in B^2(\mu)$. By definition, we have $\langle f_{\nu_1}, f_{\nu_2} \rangle_{B^2(\mu)} = \langle \text{clr}[f_{\nu_1}], \text{clr}[f_{\nu_2}] \rangle_{L^2(\mu)}$, which immediately implies that $\text{clr} : B^2(\mu) \rightarrow L_0^2(\mu)$ is isometric. We now formulate the main statement of this section:

Theorem 2.3 (Boogaart et al., 2014). *The Bayes Hilbert space $B^2(\mu)$ is a Hilbert space.*

Note that in Proposition A.2 in appendix A.1, we introduce a notion of canonical embedding, which enables us to identify the Bayes Hilbert space $B^2(\mathcal{T}_0, \mathcal{A} \cap \mathcal{T}_0, \mu)$ with a closed subspace of $B^2(\mathcal{T}, \mathcal{A}, \mu)$ for any $\mathcal{T}_0 \in \mathcal{A}$. Furthermore, we explicitly compute the orthogonal projection onto $B^2(\mathcal{T}_0, \mathcal{A} \cap \mathcal{T}_0, \mu)$. This construction is new to the best of the authors’ knowledge. An important consequence of the properties of the orthogonal projection is that we may restrict linear problems (like regression models) onto subsets of \mathcal{T} consistently with the geometry of the Bayes Hilbert spaces. For compositional data, the correspondence of subcompositions in $\mathcal{T}_0 \subset \mathcal{T}$ to subspaces of the Bayes Hilbert space is referred to as *subcompositional coherence* (Pawlowsky-Glahn et al., 2015).

3 Density-on-scalar regression

We consider regression models with a density as response and scalar covariates. More precisely, the response has to be an element of a Bayes Hilbert space $B^2(\mu) = B^2(\mathcal{T}, \mathcal{A}, \mu)$. This requires μ to be finite on $(\mathcal{T}, \mathcal{A})$, excluding, e.g., densities on the whole real line using the Lebesgue measure as reference or densities which are exactly zero in parts of \mathcal{T} . To consider $\mathcal{T} = \mathbb{R}$ with the Borel σ -algebra $\mathfrak{B}_{\mathbb{R}}$, a possible reference is the probability measure corresponding to the standard normal distribution (Boogaart et al., 2014). If a density is not directly observed but estimated from an observed sample, density values of zero can be avoided by choosing a density estimation method that yields a positive density. For discrete sets \mathcal{T} , one option is to replace observed density values of zero with small values (e.g., Pawlowsky-Glahn et al., 2015). The framework allows for a variety of different applications. Usually, we consider $\mathcal{T} \subset \mathbb{R}$ with three common cases: In the *continuous case*, we consider a nontrivial interval $\mathcal{T} = I$ with $\mathcal{A} = \mathfrak{B}$ the Borel σ -algebra restricted to I and $\mu = \lambda$ the Lebesgue measure. The *discrete case* refers to a discrete set $\mathcal{T} = \{t_1, \dots, t_D\}$ with $\mathcal{A} = \mathcal{P}(\mathcal{T})$ the power set of \mathcal{T} and $\mu = \sum_{d=1}^D w_d \delta_{t_d}$ a weighted sum of Dirac measures, where $w_d > 0$. The *mixed case* is a mixture of both: As in the continuous case, we have $\mathcal{T} = I$ and $\mathcal{A} = \mathfrak{B}$, but some points $\mathcal{D} = \{t_1, \dots, t_D\} \subset I$ have positive probability mass. The corresponding reference measure is a mixture of weighted Dirac measures and the Lebesgue measure, i.e., $\mu = \sum_{d=1}^D w_d \delta_{t_d} + \lambda$. Note that the special case $\mathcal{D} = \emptyset$ yields the continuous case. Our application in Section 4 gives an example for the mixed case.

3.1 Regression model

Density-on-scalar regression is motivated by function-on-scalar regression. Both regression types are closely related (at least in the continuous case), as density-on-scalar models can be transformed to function-on-scalar models in $L_0^2(\mu)$ via the clr transformation. We formulate our model analogously to structured additive function-on-scalar regression models (Brockhaus et al., 2015), considering densities in a Bayes Hilbert space $B^2(\mu)$ instead of functions in $L^2(I, \mathfrak{B}, \lambda)$ and using the

corresponding operations. For data pairs $(y_i, \mathbf{x}_i) \in B^2(\mu) \times \mathbb{R}^K$, $K \in \mathbb{N}$, $i = 1, \dots, N$, $N \in \mathbb{N}$, this yields the structured additive density-on-scalar regression model

$$y_i = h(\mathbf{x}_i) \oplus \varepsilon_i = \bigoplus_{j=1}^J h_j(\mathbf{x}_i) \oplus \varepsilon_i, \quad (3.1)$$

where $\varepsilon_i \in B^2(\mu)$ are functional error terms with $\mathbb{E}(\varepsilon_i) = 0 \in B^2(\mu)$ and $h_j(\mathbf{x}_i) \in B^2(\mu)$ are partial effects, $J \in \mathbb{N}$. The expectations of the $B^2(\mu)$ -valued random elements ε_i are defined using the Bochner integral (e.g., Hsing and Eubank, 2015). Each partial effect $h_j(\mathbf{x}_i) \in B^2(\mu)$ in (3.1) models an effect of none, one or more covariates in \mathbf{x}_i .

Covariate(s)	Type of effect	$h_j(\mathbf{x})$
None	Intercept	β_0
One scalar covariate x	Linear effect	$x \odot \beta$
	Flexible effect	$g(x)$
Two scalar covariates x_1, x_2	Linear interaction	$x_1 \odot (x_2 \odot \beta)$
	Functional varying coefficient	$x_1 \odot g(x_2)$
	Flexible interaction	$g(x_1, x_2)$
Grouping variable k	Group-specific intercepts	β_k
Grouping variable k and scalar x	Group-specific linear effects	$x \odot \beta_k$
	Group-specific flexible effects	$g_k(x)$

Table 3.1: Partial effects for density-on-scalar regression.

Table 3.1 gives an overview of possible partial effects, inspired by Table 1 in Brockhaus et al. (2015). The upper part shows effects for up to two different scalar covariates. In the lower part, group-specific effects for categorical variables are presented. Interactions of the given effects are possible as well. Scalar covariates are denoted by x , densities in $B^2(\mu)$ by β and $g(\cdot)$. Note that constraints are necessary to obtain identifiable models. For a model with an intercept β_0 , this is obtained by centering the partial effects:

$$\frac{1}{N} \odot \bigoplus_{i=1}^N h_j(\mathbf{x}_i) = 0. \quad (3.2)$$

More details about how to include this constraint in a functional linear array model for function-on-scalar regression can be found in appendix A of Brockhaus et al. (2015). A similar procedure can be used to obtain a centering of interaction effects around the main effects, see appendix A of Stöcker et al. (2021). Both approaches are based on Wood (2017, Section 1.8.1) and can be transferred straightforwardly to density-on-scalar regression.

3.2 Estimation by Gradient Boosting

To estimate the function $h(\mathbf{x}_i) \in B^2(\mu)$ in Equation (3.1), the sum of squared errors

$$\text{SSE}(h) := \sum_{i=1}^N \|\varepsilon_i\|_{B^2(\mu)}^2 = \sum_{i=1}^N \|y_i \ominus h(\mathbf{x}_i)\|_{B^2(\mu)}^2 = \sum_{i=1}^N \rho_{y_i}(h(\mathbf{x}_i)) \quad (3.3)$$

is minimized. Here, $\rho_{y_i} : B^2(\mu) \rightarrow \mathbb{R}$, $f_\nu \mapsto \|y_i \ominus f_\nu\|_{B^2(\mu)}^2$ is the quadratic loss functional. To simplify the minimization problem and to determine the type of an effect, compare Table 3.1, we consider a basis representation for each partial effect:

$$h_j(\mathbf{x}_i) = \left(\mathbf{b}_j(\mathbf{x}_i)^\top \otimes \mathbf{b}_Y^\top \right) \boldsymbol{\theta}_j = \bigoplus_{n=1}^{K_j} \bigoplus_{m=1}^{K_Y} b_{j,n}(\mathbf{x}_i) \odot b_{Y,m} \odot \theta_{j,n,m}, \quad (3.4)$$

where $\mathbf{b}_j = (b_{j,1}, \dots, b_{j,K_j}) : \mathbb{R}^K \rightarrow \mathbb{R}^{K_j}$ is a vector of basis functions in direction of the covariates and $\mathbf{b}_Y = (b_{Y,1}, \dots, b_{Y,K_Y}) \in B^2(\mu)^{K_Y}$ is a vector of basis functions over \mathcal{T} . With \otimes , we denote the Kronecker product of a real-valued with a $B^2(\mu)$ -valued matrix. It is defined like the Kronecker product of two real-valued matrices, using \odot instead of the usual multiplication. Similarly, matrix multiplication of a real-valued with a $B^2(\mu)$ -valued matrix is defined by replacing sums with \oplus and products with \odot in the usual matrix multiplication. Our goal is to estimate the coefficient vector $\boldsymbol{\theta}_j = (\theta_{j,1,1}, \dots, \theta_{j,K_j,K_Y}) \in \mathbb{R}^{K_j K_Y}$. To allow sufficient flexibility for h_j , the product $K_j K_Y$ can be chosen to be large. The necessary regularization can then be accomplished with a Ridge-type penalty term $\boldsymbol{\theta}_j^\top \mathbf{P}_{j,Y} \boldsymbol{\theta}_j$. For a basis representation as in equation (3.4), an anisotropic penalty matrix $\mathbf{P}_{j,Y} = \lambda_j(\mathbf{P}_j \otimes \mathbf{I}_{K_Y}) + \lambda_Y(\mathbf{I}_{K_j} \otimes \mathbf{P}_Y)$ can be used. Here, $\mathbf{P}_j \in \mathbb{R}^{K_j \times K_j}$ and $\mathbf{P}_Y \in \mathbb{R}^{K_Y \times K_Y}$ are suitable penalty matrices for \mathbf{b}_j and \mathbf{b}_Y , respectively, and $\lambda_j, \lambda_Y \geq 0$ are smoothing parameters in the respective directions. Alternatively, a simplified isotropic penalty matrix $\mathbf{P}_{j,Y} = \lambda_j((\mathbf{P}_j \otimes \mathbf{I}_{K_Y}) + (\mathbf{I}_{K_j} \otimes \mathbf{P}_Y))$ with only one smoothing parameter is possible (Brockhaus et al., 2020). The basis representation framework might seem restrictive at first, but it indeed allows for very flexible modeling of the effects, as discussed below.

We fit model (3.1) using a component-wise gradient boosting algorithm, where the expected loss is minimized step-wise along the steepest gradient descent. It is an adaption of the algorithm presented in Brockhaus et al. (2015), which was modified from Hothorn et al. (2014). Advantages of this approach are that it can deal with a large number of covariates, it performs variable selection, and includes regularization. Bühlmann and Yu (2003) discuss theoretical properties of gradient boosting w.r.t. sum of squares errors, which is typically referred to as L_2 -Boosting, for scalar responses. They show – simplifying to a single learner – that bias decays exponentially fast while estimator variance increases in exponentially small steps over the boosting iterations, which supports the general practice of stopping the algorithm early before it eventually reaches the standard (penalized) least squares estimate. Lutz and Bühlmann (2006) show consistency of component-wise L_2 -Boosting for linear regression with both high-dimensional multivariate response and predictors. Similar to these predecessors, our L_2 -Boosting algorithm for Bayes Hilbert spaces simplifies to repeated re-fitting of residuals – which, however, present densities in our case.

Algorithm: Bayes space L_2 -Boosting for density-on-scalar models

1. Select vectors of basis functions $\mathbf{b}_Y, \mathbf{b}_j$, the starting coefficient vector $\boldsymbol{\theta}_j^{[0]} \in \mathbb{R}^{K_j K_Y}$, and penalty matrices $\mathbf{P}_{j,Y}, j = 1, \dots, J$. Choose the step-length $\kappa \in (0, 1)$ and the stopping iteration m_{stop} and set the iteration number m to zero. We comment on a suitable selection of these quantities below.
2. Calculate the negative gradient of the empirical risk with respect to the Fréchet differential (see appendix A.2 for the proof of this equation)

$$U_i := \ominus \nabla \rho_{y_i}(f_\nu) \Big|_{f_\nu = \hat{h}^{[m]}(\mathbf{x}_i)} = 2 \odot \left(y_i \ominus \hat{h}^{[m]}(\mathbf{x}_i) \right), \quad (3.5)$$

where $\hat{h}^{[m]}(\mathbf{x}_i) = \bigoplus_{j=1}^J \left(\mathbf{b}_j(\mathbf{x}_i)^\top \otimes \mathbf{b}_Y^\top \right) \boldsymbol{\theta}_j^{[m]}$. Fit the base-learners

$$\hat{\gamma}_j = \underset{\gamma \in \mathbb{R}^{K_j K_Y}}{\operatorname{argmin}} \sum_{i=1}^N \left\| U_i \ominus \left(\mathbf{b}_j(\mathbf{x}_i)^\top \otimes \mathbf{b}_Y^\top \right) \gamma \right\|_{B^2(\mu)}^2 + \gamma^\top \mathbf{P}_{j,Y} \gamma \quad (3.6)$$

for $j = 1, \dots, J$ and select the best base-learner

$$j^* = \underset{j=1, \dots, J}{\operatorname{argmin}} \sum_{i=1}^N \left\| U_i \ominus \left(\mathbf{b}_j(\mathbf{x}_i)^\top \otimes \mathbf{b}_Y^\top \right) \hat{\gamma}_j \right\|_{B^2(\mu)}^2. \quad (3.7)$$

3. The coefficient vector corresponding to the best base-learner is updated, the others stay the same: $\boldsymbol{\theta}_{j^*}^{[m+1]} := \boldsymbol{\theta}_{j^*}^{[m]} + \kappa \hat{\gamma}_{j^*}$, $\boldsymbol{\theta}_j^{[m+1]} := \boldsymbol{\theta}_j^{[m]}$ for $j \neq j^*$.
4. While $m < m_{\text{stop}}$, increase m by one and go back to step 2. Stop otherwise.

The resulting estimator of model (3.1) is $\hat{y}_i = \hat{\mathbb{E}}(y_i \mid \mathbf{X} = \mathbf{x}_i) = \bigoplus_{j=1}^J \hat{h}_j^{[m_{\text{stop}}]}(\mathbf{x}_i)$, with $\hat{h}_j^{[m_{\text{stop}}]}(\mathbf{x}_i) = \left(\mathbf{b}_j(\mathbf{x}_i)^\top \otimes \mathbf{b}_Y^\top \right) \boldsymbol{\theta}_j^{[m_{\text{stop}}]}$. In the following, we discuss the selection of parameters in step 1, see also Brockhaus et al. (2015) and Brockhaus et al. (2020). The choice of vectors of basis functions \mathbf{b}_Y and \mathbf{b}_j and their corresponding penalty matrices \mathbf{P}_j and \mathbf{P}_Y depends on the desired partial effect $h_j(\mathbf{x})$. Regarding the basis functions \mathbf{b}_j in direction of the covariates, suitable selections for flexible effects are B-splines with a difference penalty. For a linear effect of one covariate, the vector of basis functions is chosen as $\mathbf{b}_j = (1, \text{id}) : \mathbb{R} \rightarrow \mathbb{R}^2$, $x \mapsto (1, x)$, resulting in the design matrix of a simple linear model. Here, a reasonable penalty matrix is $\mathbf{P}_j = \mathbf{I}_2$ corresponding to the Ridge penalty. A basis $\mathbf{b}_Y \in B^2(\mu)^{K_Y}$ can be obtained from a suitable basis $\bar{\mathbf{b}}_Y \in L^2(\mu)^{K_Y+1}$ as follows. Transforming $\bar{\mathbf{b}}_Y$ to $L_0^2(\mu)^{K_Y}$ yields a basis $\tilde{\mathbf{b}}_Y \in L_0^2(\mu)^{K_Y}$. The respective transformation matrix is constructed in appendix B. Applying the inverse clr transformation on each component of $\tilde{\mathbf{b}}_Y$ gives the desired basis \mathbf{b}_Y . For the continuous case, a reasonable choice for $\bar{\mathbf{b}}_Y \in L^2(\lambda)^{K_Y+1}$ is a B-spline basis with a difference penalty, allowing for flexible modeling of the response densities. For the discrete case, a suitable selection is $\bar{\mathbf{b}}_Y = (\mathbb{1}_{\{t_1\}}, \dots, \mathbb{1}_{\{t_D\}}) \in L^2(\sum_{d=1}^D w_d \delta_{t_d})^D$, where $\mathbb{1}_A$ denotes the indicator function of $A \in \mathcal{A}$. Again, a difference penalty can be used to control the volatility of the estimates. The mixed case is not as straightforward. We show in Section 3.3 that it can be decomposed

into a continuous and a discrete component. Thus, it is not necessary to explicitly select basis functions $\mathbf{b}_Y \in B^2(\mu)^{K_Y}$ for the mixed case. However, they can be obtained by concatenating the basis functions of the continuous and the discrete components.

Selecting the smoothing parameters is also important for regularization. They are specified such that the degrees of freedom are equal for all base-learners, to ensure a fair base-learner selection in each iteration of the algorithm. Otherwise, selection of more flexible base-learners is more likely than that of less flexible ones, see Hofner et al. (2011). However, the effective degrees of freedom of an effect after m_{stop} iterations will in general differ from those preselected for the base learners in each single iteration. They are successively adapted to the data. The starting coefficient vectors $\boldsymbol{\theta}_j^{[0]}$ are usually all set to zero, enabling variable selection as an effect that is never selected stays at zero. Like in functional regression, a suitable offset can be used for the intercept to improve the convergence rate of the algorithm, e.g., the mean density of the responses in $B^2(\mu)$. Note that a scalar offset, which is another common choice in functional regression, equals zero in the Bayes Hilbert space and thus corresponds to no offset. The optimal number of boosting iterations m_{stop} can be found with cross-validation, sub-sampling or bootstrapping, with samples generated on the level of elements of $B^2(\mu)$. The early-stopping avoids overfitting. Finally, the value $\kappa = 0.1$ for the step-length is suitable in most applications for a quadratic loss function (Brockhaus et al., 2020). A smaller step-length usually requires a larger value for m_{stop} .

Note that the estimation problem can also be solved in $L_0^2(\mu)$ based on the clr transformed model, with the estimates in $B^2(\mu)$ obtained applying the inverse clr transformation, as proposed by Talská et al. (2018) for functional linear models on closed intervals. For our functional additive models, gradient boosting can be performed in $L_0^2(\mu)$ analogously to the algorithm described above. The results of both algorithms are equivalent via the clr transformation, which we show in appendix C. In the continuous case, this yields the functional boosting algorithm of Brockhaus et al. (2015) with the modification that the basis functions \mathbf{b}_Y are constrained to be elements of $L_0^2(\lambda)$ instead of $L^2(\lambda)$.

3.3 Estimation in the mixed case

Recall the mixed case, i.e., $B^2(\mu) = B^2(I, \mathfrak{B}, \mu)$ with $\mu = \delta + \lambda$, where $\delta = \sum_{d=1}^D w_d \delta_{t_d}$ for $\{t_1, \dots, t_D\} = \mathcal{D} \subset I$ and $w_d > 0$. Due to the mixed reference measure, the specification of suitable basis functions $\mathbf{b}_Y \in B^2(\mu)^{K_Y}$ is not straightforward. We simplify this by tracing the estimation problem back to two separate estimation problems – one continuous and one discrete. For the continuous one, consider the Bayes Hilbert space $B^2(\lambda) = B^2(\mathcal{C}, \mathfrak{B} \cap \mathcal{C}, \lambda)$, where $\mathcal{C} := I \setminus \mathcal{D} \in \mathfrak{B}$. Remarkably, its orthogonal complement in $B^2(\mu)$ is not the Bayes Hilbert space $B^2(\mathcal{D}, \mathfrak{B} \cap \mathcal{D}, \delta)$. Instead, an additional arbitrary discrete value $t_{D+1} \in \mathbb{R} \setminus \mathcal{D}$ is required, which can be considered the discrete equivalent of \mathcal{C} . Thus, an intuitive choice is $t_{D+1} \in \mathcal{C}$. Then, the orthogonal complement of $B^2(\lambda)$ in $B^2(\mu)$ is the Bayes Hilbert space $B^2(\delta^\bullet) = B^2(\mathcal{D}^\bullet, \mathcal{P}(\mathcal{D}^\bullet), \delta^\bullet)$, where $\mathcal{D}^\bullet := \mathcal{D} \cup \{t_{D+1}\}$ and $\delta^\bullet := \sum_{d=1}^{D+1} w_d \delta_{t_d}$ with $w_{D+1} := \lambda(I)$. The embeddings to consider $B^2(\lambda)$ and

$B^2(\delta^\bullet)$ as subspaces of $B^2(\mu)$ are $\iota_c : B^2(\lambda) \hookrightarrow B^2(\mu)$ and $\iota_d : B^2(\delta^\bullet) \hookrightarrow B^2(\mu)$, which are defined as $\iota_c(f_c) = f_c$ and $\iota_d(f_d) = f_d(t_{D+1})$ on \mathcal{C} , respectively, and $\iota_c(f_c) = \exp \mathcal{S}_\lambda(f_c)$ and $\iota_d(f_d) = f_d$ on \mathcal{D} . Here, $\mathcal{S}_\lambda(f_c)$ is the mean logarithmic integral as defined in (2.1). Note that $\exp \mathcal{S}_\lambda(f_c)$ corresponds to the geometric mean of f_c using the natural generalization of the usual definition of the geometric mean of a discrete set $\{g(s_1), \dots, g(s_L)\}$, since $(\prod_{l=1}^L g(s_l))^{1/L} = \exp \mathcal{S}_{B^2(\mathcal{T}, \mathcal{P}(\mathcal{T}), \sum_{l=1}^L \delta_{s_l})}(g)$ for $\mathcal{T} = \{s_1, \dots, s_L\}$. For $f \in B^2(\mu)$, the unique functions $f_c \in B^2(\lambda)$, $f_d \in B^2(\delta^\bullet)$ such that $f = \iota_c(f_c) \oplus \iota_d(f_d)$ are given by

$$f_c : \mathcal{C} \rightarrow \mathbb{R}, \quad t \mapsto f(t), \quad f_d : \mathcal{D}^\bullet \rightarrow \mathbb{R}, \quad t \mapsto \begin{cases} 1, & t = t_{D+1} \\ \frac{f(t)}{\exp \mathcal{S}_\lambda(f)}, & t \in \mathcal{D}. \end{cases} \quad (3.8)$$

See Proposition A.3 in appendix A.2 for the proof that the orthogonal complement of $B^2(\lambda)$ in $B^2(\mu)$ is $B^2(\delta^\bullet)$, including (3.8). Then, we obtain $\|f\|_{B^2(\mu)}^2 = \|f_c\|_{B^2(\lambda)}^2 + \|f_d\|_{B^2(\delta^\bullet)}^2$ implying that minimizing the sum of squared errors (3.3) is equivalent to minimizing its discrete and continuous components separately and then combining the solutions \hat{f}_c and \hat{f}_d in the overall solution $\hat{f} = \iota_c(\hat{f}_c) \oplus \iota_d(\hat{f}_d)$.

Equivalently, we can decompose the Hilbert space $L_0^2(I, \mathfrak{B}, \mu)$ such that embeddings and clr transformations commute. See Proposition A.4 in appendix A.2 for details and proof.

3.4 Interpretation

The interpretation of the estimated effects $\hat{h}_j := \hat{h}_j^{[m_{\text{stop}}]}(\mathbf{x}_i) \in B^2(\mu)$, $j = 1, \dots, J$, has to respect the special structure of Bayes Hilbert spaces. In particular, it should be independent of the selected representative of an equivalence class in $B^2(\mu)$. Naturally, interpretation in a Bayes Hilbert space is relative. Accordingly, the shape of clr transformed effects can be interpreted using differences, resulting in an interpretation analogous to the well-known odds ratios. For two effects \hat{h}_j and \hat{h}_k for $j \neq k \in \{1, \dots, J\}$ and $s, t \in \mathcal{T}$, we have

$$\exp \left(\text{clr}[\hat{h}_j](t) - \text{clr}[\hat{h}_j](s) - \left(\text{clr}[\hat{h}_k](t) - \text{clr}[\hat{h}_k](s) \right) \right) = \frac{\hat{h}_j(t) / \hat{h}_j(s)}{\hat{h}_k(t) / \hat{h}_k(s)}. \quad (3.9)$$

The compound fraction on the right is called *odds ratio of \hat{h}_j and \hat{h}_k for t compared to s* , its numerator is called *odds of \hat{h}_j for t compared to s* . Thus, the log odds ratio corresponds to the difference of the differences of the clr transformed effects evaluated at t and s . In a reference coding setting, this reduces to a simple difference as the clr transformed effect for the reference category is 0. Considering additional effects $\hat{h}_{\mathcal{J}} = \bigoplus_{l \in \mathcal{J}} \hat{h}_l$ with $\mathcal{J} \subset \{1, \dots, J\} \setminus \{j, k\}$, the odds ratio of $\hat{h}_{\mathcal{J}} \oplus \hat{h}_j$ and $\hat{h}_{\mathcal{J}} \oplus \hat{h}_k$ for t compared to s is equal to the odds ratio of \hat{h}_j and \hat{h}_k for t compared to s , enabling a *ceteris paribus* interpretation.

The odds ratio (3.9) is a ratio of density values, which depending on the case (discrete, continuous, mixed) is identical to or approximates a usual ratio of probabilities: Let $\mathbb{P}_j \cong \hat{h}_j$ and $\mathbb{P}_k \cong \hat{h}_k$ be the corresponding probability measures in $B^2(\mu)$ of the estimated effects. In the discrete case, i.e., $\mathcal{T} = \{t_1, \dots, t_D\}$ and

$\mu = \sum_{d=1}^D w_d \delta_{t_d}$, we have $\mathbb{P}_j(\{t_d\})/\mu(\{t_d\}) = [w_d \hat{h}_j(t_d)]/w_d = \hat{h}_j(t_d)$ for every $t_d \in \mathcal{T}$. Then, the odds ratio of \hat{h}_j and \hat{h}_k for $t_{d_1} \in \mathcal{T}$ compared to $t_{d_2} \in \mathcal{T}$ equals $[\mathbb{P}_j(\{t_{d_1}\})/\mathbb{P}_j(\{t_{d_2}\})] / [\mathbb{P}_k(\{t_{d_1}\})/\mathbb{P}_k(\{t_{d_2}\})]$, i.e., the odds ratio of \mathbb{P}_j and \mathbb{P}_k for $\{t_{d_1}\}$ compared to $\{t_{d_2}\}$. In the continuous and mixed cases, i.e., $\mathcal{T} = I \subset \mathbb{R}$ and $\mu = \sum_{d=1}^D w_d \delta_{t_d} + \lambda$ for $\mathcal{D} = \{t_1, \dots, t_D\} \subset I$ (continuous case: $\mathcal{D} = \emptyset$), the relation holds approximately: For $s, t \in I$, let $A_n, B_n \subseteq I$ be two nested sequences of intervals centered at s and t for all $n \in \mathbb{N}$, whose intersection is $\{s\}$ and $\{t\}$, respectively. Then,

$$\frac{\hat{h}_j(t)}{\hat{h}_j(s)} = \lim_{n \rightarrow \infty} \frac{\mathbb{P}_j(B_n) / \mu(B_n)}{\mathbb{P}_j(A_n) / \mu(A_n)} \quad \text{and thus} \quad \frac{\hat{h}_j(t) / \hat{h}_j(s)}{\hat{h}_k(t) / \hat{h}_k(s)} = \lim_{n \rightarrow \infty} \frac{\mathbb{P}_j(B_n) / \mathbb{P}_j(A_n)}{\mathbb{P}_k(B_n) / \mathbb{P}_k(A_n)}, \quad (3.10)$$

i.e., the odds ratio of density values approximates the odds ratio of probabilities for small neighborhoods of s and t . We prove (3.10) in appendix A.2, where we also show that if there exist $I_t, I_s \subset I$ with $\hat{h}_j(t)/\hat{h}_j(s) < \hat{h}_k(t)/\hat{h}_k(s)$ for all $t \in I_t, s \in I_s$, then, $\mathbb{P}_j(I_t)/\mathbb{P}_j(I_s) < \mathbb{P}_k(I_t)/\mathbb{P}_k(I_s)$. Further ideas of interpreting effects are developed in appendix D.

4 Application

With our modeling approach, we analyze the distribution of the female share in a couple's total labor income in Germany. Note that for simplicity we use the terms East/West Germany also after reunification. Although we refer to Bertrand et al. (2015), we do not focus on the question of whether there is actually a decline in density at 0.5.

4.1 Background and hypotheses

There is a larger share fraction in Germany below 0.5 (as in Bertrand et al., 2015) reflecting the gender pay gap, but there is no consensus in the literature regarding a discontinuous drop at 0.5 (Sprengholz et al., 2020; Kuehnle et al., 2021). The employment and earnings of female partners show a strong childhood penalty (Kleven et al., 2019; Fitzenberger et al., 2013). The social norm in West Germany used to be that mothers should stay at home with their children. Institutionalized child care was scarce and there are strong financial incentives for part-time work for the second earner. Together, this results in part-time employment increasing strongly for women after having their first child. Thus, we expect that the income share of the woman is lower in the presence of children reflecting a childhood penalty.

Due to changing social norms, the female employment increases strongly over time. However, occupational segregation by gender is persistent (Cortes and Pan, 2018) with men being more likely to work in better paying occupations. Still, occupations with a higher share of women seem to benefit from technological change (Black and Spitz-Oener, 2010). Thus, the income share of female partners without children is predicted to grow over time.

Ex ante reasoning suggests an ambiguous effect on the childhood penalty. On the one hand, the incentives for part-time work especially for female partners with young children may prevent an increase in the income share. Thus, the childhood penalty in the income share may even grow over time. On the other hand, growing female employment may actually increase the female income share, especially among female partners with older children.

Turning to the comparison between East and West Germany, the literature emphasizes that social norms are likely to differ between the two parts of the country (Beblo and Gorges, 2018). Before reunification, it was basically mandatory for women to work in East Germany and comprehensive institutionalized child care was available. This suggests that the female income share in East Germany is higher than in West Germany.

After reunification, social norms have been converging between the East and the West. In East Germany, female employment may have fallen more strongly than for males due to the strong economic transformation and the lower mobility of female partners after job loss. Part-time employment is likely to become more prevalent in East Germany, and over time mothers more often drop out of the labor force. While we expect the childhood penalty to be lower in East Germany than in West Germany, it is ex ante ambiguous whether the East-West gap in the childhood penalty decreases over time, a question of interest.

4.2 Data and descriptive evidence on response densities

Our data set derived from the German Socio-Economic Panel (see appendix E for details) contains 154,924 observations of couples of opposite sex living together in a household, where at least one partner reports positive labor income. We include cohabitating couples in addition to married ones as there is a strong tax incentive to get married in case of unequal incomes, leading to a bias. The women's *share* in the couple's total gross labor income together with the household's sample *weight* yields the response densities. Four variables serve as covariates. First, the binary covariate *West_East* specifies whether the couple lives in *West* Germany or in *East* Germany (including Berlin). A second finer disaggregation distinguishes six *regions* (two in *East* and four in *West* Germany, see appendix E.1). The third covariate *c_age* is a categorical variable for the age range (in years) of the couple's youngest child living in the household: *0-6*, *7-18*, and *other* (i.e., couples without minor children). Finally, *year* ranges from 1984 (*West* Germany)/1991 (*East* Germany) to 2016.

A response density $f_{region, c_age, year} : [0, 1] \rightarrow \mathbb{R}^+$, $s \mapsto f_{region, c_age, year}(s)$ is estimated for each combination of covariate values (note that *region* determines *West_East*), with s denoting the woman's income share. In total, this yields 552 response densities. Often, we just write f and omit the indices. Before elaborating on the estimation, we determine a suitable underlying Bayes Hilbert space $B^2(\mu) = B^2(\mathcal{T}, \mathcal{A}, \mu)$. Since s denotes a share, we consider $\mathcal{T} = [0, 1]$ with $\mathcal{A} = \mathfrak{B}$. The Lebesgue measure is no appropriate reference, as the boundary values 0 and 1 correspond to single-earner households and thus have positive probability mass (see appendix E.2 for exemplary barplots). A suitable reference measure respecting this structure is $\mu := \delta_0 + \lambda + \delta_1$, i.e., the mixed case with $D = 2$, $t_1 = 0$, $t_2 = 1$, and $w_1 = 1 = w_2$,

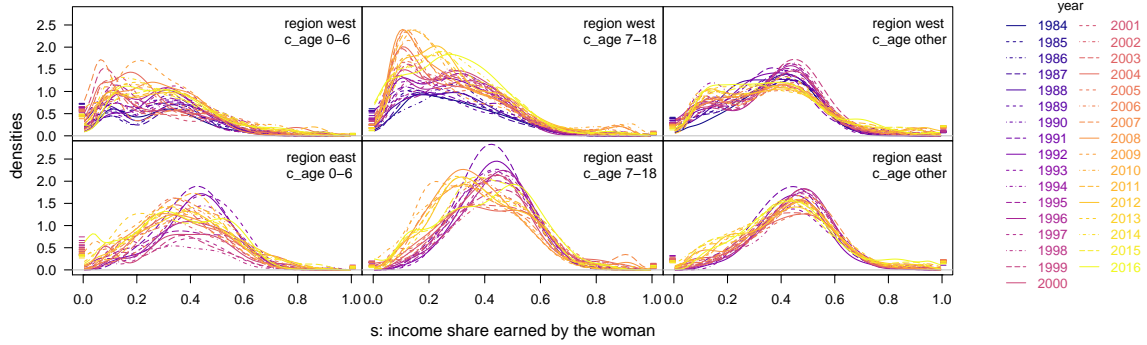


Figure 4.1: Response densities for *regions west* and *east* [rows] for all three values of *c_age* [columns].

see Section 3. The values $f(0)$ and $f(1)$ are the (weighted) relative frequencies for shares of 0 and 1, denoted by p_0 and p_1 , respectively. To estimate f on $(0, 1)$, we compute continuous densities based on dual-earner households, and multiply them by $p_{(0,1)} = 1 - p_0 - p_1$. For this purpose, weighted kernel density estimation with beta-kernels (Chen, 1999) is used to preserve the support $(0, 1)$, see appendix E.3 for details.

The response densities are very similar in the different *regions* within *West* and *East* Germany, respectively. Thus, we restrict visualization in Figure 4.1 to the exemplary *regions west* (North Rhine-Westphalia) for *West* Germany and *east* (Saxony-Anhalt, Thuringia, Saxony) for *East* Germany. See Figure E.7 in appendix E.4 for the corresponding figure for all six *regions*, with additional illustration of the respective relative frequencies p_0 , $p_{(0,1)}$, p_1 over time. Figure 4.1 depicts the response densities for all *years* by the *c_age* groups, for the *regions west* and *east*, with a color gradient and different line types distinguishing the *year*. The density values $f(0)$ and $f(1)$ are represented as dashes, shifted slightly outwards for better visibility. Consider the continuous parts ($s \in (0, 1)$): In *west* (first row), the densities differ between couples with $(0-6$ and $7-18)$ and without minor children (*other*), with the latter lying more to the right reflecting lower female shares in the presence of children. In *east*, the shapes are more egalitarian and vary much less with the age of the youngest child. In all cases, the fraction of couples with a share less than 0.5 exceeds the fraction with a share larger than 0.5. Over time, the probability mass for a small share increases and the share of non-working women declines, reflecting the increase in female part-time employment. These findings show the importance of considering the mixed densities. The shares of dual-earner households and non-working women evolve in opposite direction over time, while the share of single-earner women remains small.

4.3 Model specification

Based on the empirical response densities $f_{region, c_age, year}$, we estimate the model

$$\begin{aligned} f_{region, c_age, year} = & \beta_0 \oplus \beta_{West_East} \oplus \beta_{region} \oplus \beta_{c_age} \oplus \beta_{c_age, West_East} \\ & \oplus g(year) \oplus g_{West_East}(year) \oplus g_{c_age}(year) \\ & \oplus g_{c_age, West_East}(year) \oplus \varepsilon_{region, c_age, year}. \end{aligned} \quad (4.1)$$

All summands are densities of the share $s \in [0, 1]$ and elements of the Bayes Hilbert space $B^2(\mu)$. The model is reference coded with reference categories $West_East = West$, $c_age = other$, and $year = 1991$. The corresponding effect for the reference is given by the intercept β_0 . The effect for the six regions β_{region} is centered around the respective β_{West_East} . The smooth year effect $g(year)$ describes the deviation for each $year$ from the reference 1991 (for $West$ Germany and $c_age other$). Finally, several interaction terms are included with a group-specific intercept $\beta_{c_age, West_East}$ as well as group-specific flexible terms $g_{West_East}(year)$, $g_{c_age}(year)$, and $g_{c_age, West_East}(year)$. They are constrained to be orthogonal to the respective main effects using a similar constraint as (3.2) to ensure identifiability. Due to reference coding, all partial effects for the reference categories are zero.

As described in Section 3.3, we decompose the Bayes Hilbert space $B^2(\mu)$ into two orthogonal subspaces $B^2(\lambda) = B^2((0, 1), \mathfrak{B} \cap (0, 1), \lambda)$ and $B^2(\delta^\bullet) = B^2(\mathcal{D}^\bullet, \mathcal{P}(\mathcal{D}^\bullet), \delta^\bullet)$, where $\mathcal{D}^\bullet = \{t_1, t_2, t_3\}$ and $\delta^\bullet = \sum_{d=1}^3 \delta_{t_d}$. We choose $t_3 = 1/2$ to represent the continuous component in between the boundary values $t_1 = 0$ and $t_2 = 1$. For every f we generate the unique functions $f_c \in B^2(\lambda)$ and $f_d \in B^2(\delta^\bullet)$ as in (3.8). As proposed in Section 3.2, we choose transformed cubic B-splines as basis functions \mathbf{b}_Y for the continuous component and a transformed basis of indicator functions for the discrete component. The remaining specification is identical in both models. We use an anisotropic penalty without penalizing in direction of the share, i.e., $\lambda_Y = 0$, to ensure the necessary flexibility towards the boundaries. For the flexible nonlinear effects, the selected basis functions are cubic B-splines with penalization of second order differences. We set the degrees of freedom to 2 for all effects but β_0 and β_{West_East} , as these only allow for a maximum value of 1. Regarding base-learner selection, β_{West_East} thus is at a slight disadvantage compared to other main effects. However, in a sensitivity check imposing equal degrees of freedom for all base-learners by adjusting λ_Y to 1 for all effects, we do not observe large deviations in the selection frequencies while the fit to the data is better with unequal degrees of freedom, see appendix E.4. Note that the intercept as well as the interaction effects are separated from the main effects due to the orthogonalizing constraints, ensuring a fair selection for the remaining base-learners. The starting coefficients are set to zero in every component and we set the step-length κ to 0.1. We obtain a stopping iteration value of 262 for the continuous model and 731 for the discrete model based on 25 bootstrap samples, respectively.

4.4 Regression Results

All effects in our regression model (4.1) are selected by the algorithm (see appendix E.5). The predictions in Figure E.8 in appendix E.4 mostly show a good fit.

In the following, we discuss the key findings.

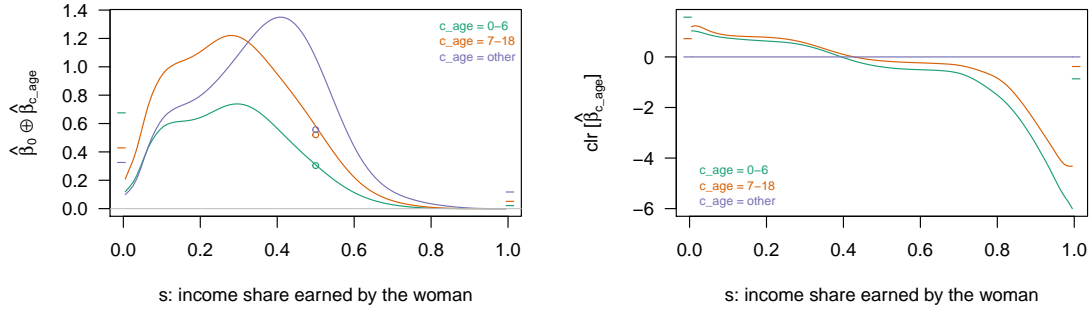


Figure 4.2: Expected densities for couples living in *West* Germany in 1991 for all three values of c_age [left] and clr transformed estimated effects of c_age [right].

The left part of Figure 4.2 shows the perturbation of the intercept by the c_age effect, i.e., the expected densities for couples without minor children (c_age *other*), for couples with children aged $0-6$, and for couples with children aged $7-18$ living in *West* Germany in 1991. The circles at 0.5 represent the expected relative frequency of dual-earner households. Our main finding is that the expected density on $(0, 1)$ for c_age *other* is unimodal with a maximum above 0.4, while the densities for c_age $0-6$ and $7-18$ are bimodal with both maxima to the left of 0.4. The latter show a similar shape, but are scaled differently. The relative frequencies of dual-earner households (circles at 0.5) and the two types of single-earner households (dashes at 0, 1) are similar for couples with children aged $7-18$ years and couples without minor children, respectively. In contrast, the relative frequency of non-working women is much higher and the relative frequency of dual-earner households is much lower for couples with children aged $0-6$. The right part of the figure shows the clr transformed effect for interpretation via (log) odds ratios, see Section 3.4. As $c_age=other$ is the reference category, we have $\text{clr}[\hat{\beta}_{other}] = 0$. The clr transformed effects of c_age $0-6$ and $7-18$ again show similar shapes on $(0, 1)$, but shifted vertically. As the log odds ratio of $\hat{\beta}_k$ and $\hat{\beta}_{other}$ for s compared to t corresponds to vertical differences within $\text{clr}[\hat{\beta}_k]$, $k \in \{0-6, 7-18\}$, the log odds ratio of $\hat{\beta}_{0-6}$ and $\hat{\beta}_{other}$ is similar to the one of $\hat{\beta}_{7-18}$ and $\hat{\beta}_{other}$. This implies they have similar impact on the shape of a density. Both log odds ratios are always negative for $s < t \in (0, 1)$, i.e., the odds for a larger versus a smaller income share are always smaller for couples with minor children than for couples without minor children, reflecting the strong childhood penalty in *West* Germany in 1991. See Appendix E.5 for quantitative examples of concrete odds ratios.

Figure 4.3 shows the expected densities for four selected *years*, separately for couples with and without minor children (see Figure E.16 in appendix E.5 for all *years*). For *other*, the frequency of non-working women ($s = 0$) falls continuously over time and the density becomes more dispersed with a lower maximum around 0.4 in 2016 than in 1993 and 2003 (however, it was even lower in 1984). In fact, by 2016 the expected density tends to have a second maximum further left and a heavier tail on the right, most likely due to the strong growth of part-time employment even among women without minor children. Furthermore, the frequency of single-earner

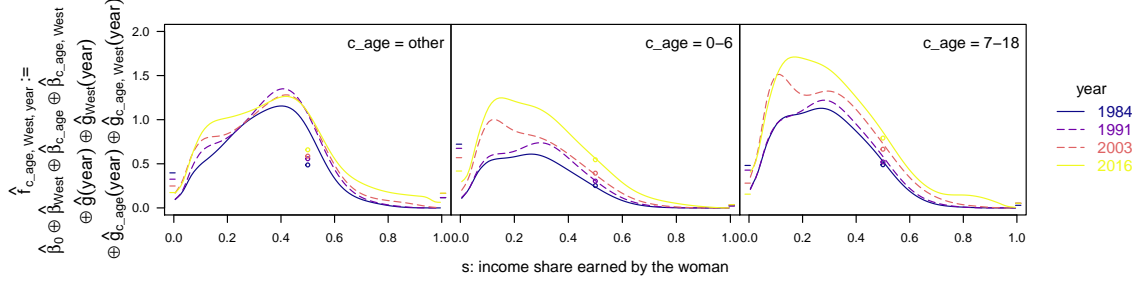


Figure 4.3: Expected densities in the *years* 1984, 1991, 2003, and 2016 for *West* Germany for all three values of c_age : *other* [left], *0-6* [middle], *7-18* [right].

women ($s = 1$) increases to a level similar to the frequency of non-working women. For *0-6* and *7-18*, we also observe a fall in the frequency of non-working women and a stronger concentration around the larger mode until 1991. However, up to 2016 the distributions show more probability mass for small shares, reflecting the even larger growth of part-time employment among women with minor children.

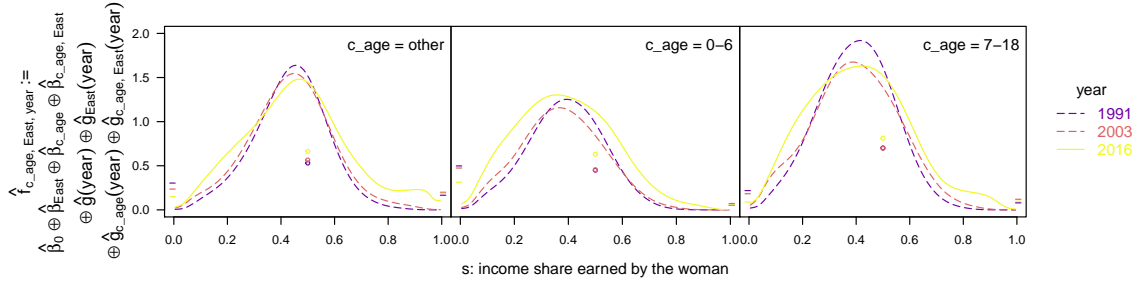


Figure 4.4: Expected densities in the *years* 1991, 2003, and 2016 for *East* Germany for all three values of c_age : *other* [left], *0-6* [middle], *7-18* [right].

Figure 4.4 shows the expected densities in *East* Germany for selected *years* (see Figure E.16 in appendix E.5 for all *years*). In all three cases, the share distribution has a unique mode at or above 0.4. The distribution becomes more dispersed over time, with more probability mass moving to the left and a growing right tail. The frequency of non-working women is falling over time. While showing a similar trend as in *West* Germany, there remain persistent differences. In *East* Germany, the frequency of non-working women for couples with minor children remains much lower and the shape of the distribution shows no trend towards a second maximum at a low share. Hence, there remains a considerable West-East gap in the childhood penalty.

To address this issue explicitly, the West-East gap in the childhood penalty is calculated by the difference-in-differences (DiD) effect for $year \in \{1991, 2016\}$ and $c_age \in \{0-6, 7-18\}$:

$$DiD_{c_age, year} = (\hat{f}_{c_age, West, year} \ominus \hat{f}_{other, West, year}) \ominus (\hat{f}_{c_age, East, year} \ominus \hat{f}_{other, East, year}).$$

Figure 4.5 shows the log odds

$$LO_{c_age, year}(t, s) := \log ([DiD_{c_age, year}](t) / [DiD_{c_age, year}](s))$$

of $DiD_{c_age, year}$ for t compared to s for pairs $(t, s) \in [0, 1]^2$, see Section 3.4, as heat maps. We omit the index $c_age, year$ in the following. The inner quadrant shows the respective heat map for $t, s \in (0, 1)$. The log odds involving the two mass points 0 and 1 are given by the band around the inner quadrants. The top-left corner concerns the log odds for $t = 0$ (non-working woman) compared to $s = 1$ (single-earner woman). The inner bands around the inner quadrant correspond to the log odds between a mass point 0, 1 and a share in $(0, 1)$. The outer bands show the constant log odds between one of the mass points and the event dual-earner household ($0 < s, t < 1$). A positive (negative) value implies that the log odds for shares t versus s are higher (lower) in the *West* than in the *East*. Thus, $LO(t, s) > 0$ for $t < s$ implies that the child penalty (lower share t is more likely relative to s in the presence of children) is more pronounced (stronger) in the *West* than in the *East*. For 1991, the vertical band for $t = 0$ to the left of the heatmap is quite red ($LO(0, s) > 0$), implying that it is much more likely that women in the *West* compared to the *East* stop working in the presence of a child, relative to all other shares. This holds both for c_age 0-6 (top panel) and c_age 7-18 (bottom panel). However, the entire heatmap shows positive (negative) values above (below) the 45-degree-line implying that the shift to lower shares compared to higher shares in the presence of children is stronger in the *West* than in the *East*, with the West-East gap in the child penalty being even larger for c_age 7-18.

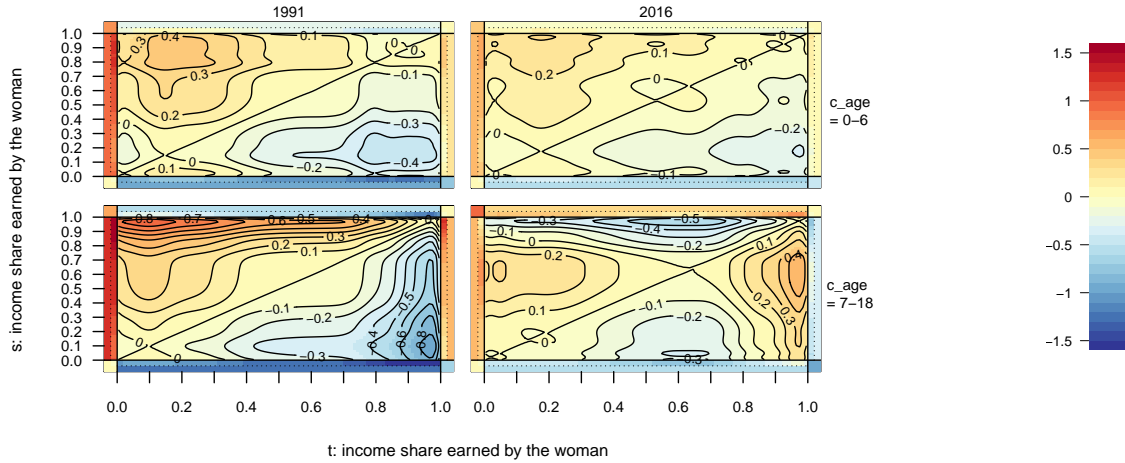


Figure 4.5: Log Odds $LO_{c_age, year}(t, s)$ of the West-East gap in the childhood penalty (DiD effects) for c_age 0-6 [top] and 7-18 [bottom] for the *years* 1991 [left] and 2016 [right].

The comparison between the two years is informative about the change in the West-East gap in the childhood penalty over time. In 2016, the childhood penalty remains larger in the *West* compared to the *East* over almost the entire share distribution – only for c_age 7-18 is there a reversal for very large shares compared to medium share levels. However, since the absolute log odds have become much smaller, especially for non-working women, the West-East gap in the childhood penalty has decreased considerably over time.

Summarizing our main findings, the frequency of non-working women and women with a lower income share is higher in *West* Germany than in *East* Germany and

these differences are larger for couples with children. Over time, the share of non-working women decreased. Among dual-earner households the dispersion of the share distribution increased over time with both a growing lower and higher tail. Despite persistent East-West differences in the share distributions and the child penalty until the end of the observation period, the West-East gap in the childhood penalty fell considerably over time.

5 Simulation study

The gradient boosting approach has already been tested extensively in several simulation studies for scalar and functional data (e.g., Brockhaus et al. (2015) and references therein). For completeness and to validate our modified approach for density-on-scalar models, we present a small simulation study for this case. It is based on the results of our analysis in Section 4. The predictions obtained there serve as true mean response densities for the simulation and are denoted by $F_i \in B^2(\mu)$, $i = 1, \dots, 552$, where each i corresponds to one combination of values for the covariates *region*, *c_age*, and *year* and $B^2(\mu)$ is the Bayes Hilbert space from Section 4. To simulate data, we perform a functional principal component (PC) analysis (e.g. Ramsay and Silverman, 2005) on the clr transformed functional residuals $\text{clr}[\hat{\varepsilon}_i] = \text{clr}[f_i \ominus F_i] = \text{clr}[f_i] - \text{clr}[F_i]$, with $f_i \in B^2(\mu)$ the response densities from the application. Let ψ_m denote the PC functions corresponding to the descending ordered eigenvalues ξ_m and let ρ_{im} denote the PC scores for $i = 1, \dots, 552$ and $m \in \mathbb{N}$. Then, the truncated Karhunen-Loève expansion for $M \in \mathbb{N}$ yields an approximation of the functional residuals: $\text{clr}[\hat{\varepsilon}_i] \approx \sum_{m=1}^M \rho_{im} \psi_m$. The PC scores can be viewed as realizations of uncorrelated random variables ρ_m with zero-mean and covariance $\text{Cov}(\rho_m, \rho_n) = \xi_m \delta_{mn}$, where δ_{mn} denotes the Kronecker delta and $m, n = 1, \dots, M$. We simulate residuals $\tilde{\varepsilon}_i$ by drawing uncorrelated random $\tilde{\rho}_{im}$ from mean zero normal distributions with variance ξ_m and applying the inverse clr transformation to the truncated Karhunen-Loève expansion, $\tilde{\varepsilon}_i = \text{clr}^{-1}[\sum_{m=1}^M \tilde{\rho}_{im} \psi_m] = \bigoplus_{m=1}^M \tilde{\rho}_{im} \odot \text{clr}^{-1}[\psi_m]$. Adding these to the mean response densities yields the simulated data: $\tilde{f}_i = F_i \oplus \tilde{\varepsilon}_i$, $i = 1, \dots, 552$. Using these as observed response densities, we then estimate model (4.1) and denote the resulting predictions with $\hat{f}_i \in B^2(\mu)$, $i = 1, \dots, 552$. We replicate this approach 200 times with $M = 102$, which is the maximal possible value due to the number of available grid points per density.

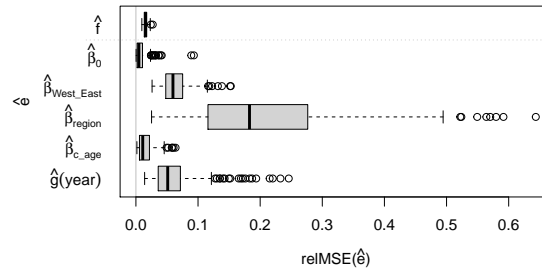


Figure 5.1: RelMSE for predictions [top] and main effects [bottom].

To evaluate the goodness of the estimation results, we use the relative mean squared error (relMSE; defined in appendix F.1) motivated by Brockhaus et al. (2015), standardizing the mean squared error with respect to the global variability of the true density. Figure 5.1 shows the boxplots of the relMSEs (200 each) of the predictions and the main effects. All effects are illustrated in appendix F.2. The distribution of $\text{relMSE}(\hat{f})$ over the 200 simulation runs shows good estimation quality, with a median of 1.55%. Regarding the main effects, the relMSEs are the smallest for $\hat{\beta}_0$ and $\hat{\beta}_{c_age}$ with medians of 0.48% and 1.1%, respectively. For $\hat{\beta}_{West_East}$ and $\hat{g}(year)$, the values tend to be slightly larger (medians: 5.96% and 5.12%) while they are clearly larger for $\hat{\beta}_{region}$ (median: 18.28%). However, the larger relative values, especially for $\hat{\beta}_{region}$, arise from the variability of the true effects being small, not from the mean squared errors being large. This is also the case for the interaction effects, see appendix F.2. Regarding model selection, the main effects are all selected in each simulation run, while the smaller interaction effects are not, see appendix F.3 for details. Overall, the estimates capture the true means F_i and all effects that are pronounced very well. Small effects in the model are estimated well in absolute, but badly in relative terms.

6 Conclusion

We presented a flexible framework for density-on-scalar regression models by formulating them in a Bayes Hilbert space $B^2(\mu)$, which respects the nature of probability densities and allows for a unified treatment of arbitrary finite measure spaces. This covers in particular the common discrete, continuous, and mixed cases. To estimate the covariate effects in $B^2(\mu)$, we introduced a gradient boosting algorithm. We used our approach to analyze the distribution of the woman’s share in a couple’s total labor income, an example of the challenging mixed case, for which we developed a decomposition into a continuous and a discrete estimation problem. We observe strong differences between West and East Germany and between couples with and without children. Among dual-earner households the dispersion of the share distribution increased over time. Despite persistent East-West differences in the share distributions and the child penalty until the end of the observation period, the West-East gap in the childhood penalty fell considerably over time. Finally, we performed a small simulation study justifying our approach in a setting motivated by our application.

Density regression has particular advantages in terms of interpretation compared to approaches considering equivalent functions like quantile functions (e.g., Yang et al., 2018; Koenker, 2005) or distribution functions (CTMs, e.g., Hothorn et al., 2014; distribution regression, e.g., Chernozhukov et al., 2013), as shifts in probability masses or bimodality are easily visible in densities. Odds-ratio-type interpretations of effect functions further add to the interpretability of our model. A crucial part in our approach is played by the clr transformation, which simplifies among other things estimation, as gradient boosting can be performed equivalently on the clr transformed densities in $L_0^2(\mu)$. This allows taking advantage of and extending existing implementations for function-on-scalar regression like the R add-on package *FDboost* (Brockhaus and Rügamer, 2018), see the github repository *FDboost* for

our enhanced version of the package and in particular our vignette “density-on-scalar_birth”. The idea to transform the densities to (a subspace of) the well-known L^2 space with its metric is also used by other approaches. Besides the clr transformation, the square root velocity transformation (Srivastava et al., 2007) as well as the log hazard and log quantile density transformations (e.g., Han et al., 2020) are popular choices. The approach of Petersen and Müller (2019) does not use a transformation, but also computes the applied Wasserstein metric via the L^2 metric. What is special about the clr transformation based Bayes Hilbert space approach, is the embedding of the untransformed densities in a Hilbert space structure. It is the extension of the well-established Aitchison geometry (Aitchison, 1986), which provides a reasonable framework for compositional data – the discrete equivalent of densities – fulfilling appealing properties like subcompositional coherence. The clr transformation helps to conveniently interpret covariate effects via ratios of density values (odds-ratios), which approximate or are equal to ratios of probabilities in three common cases (discrete, continuous, mixed). Modeling those three cases in a unified framework is a novelty to the best of the authors’ knowledge, and a contribution of our approach to the literature on density regression.

Due to the gradient boosting algorithm used for estimation, our method includes variable selection and regularization, while it can deal with numerous covariates. However, like all gradient boosting approaches, it is limited by not naturally yielding inference – unlike some existing approaches (e.g., Petersen and Müller, 2019). This might be developed using a bootstrap-based approach or selective inference (Rügamer and Greven, 2020) in the future. Alternatively, other estimation methods allowing for formal inference could be derived.

The (current) definition of Bayes Hilbert spaces, which only allows finite reference measures, does not cover the interesting case of the measurable space $(\mathbb{R}, \mathfrak{B}_{\mathbb{R}})$ with Lebesgue measure λ . Though $(\mathbb{R}, \mathfrak{B}_{\mathbb{R}})$ can still be considered using, e.g., the probability measure corresponding to the standard normal distribution (Boogaart et al., 2014) as reference, it would be desirable to extend Bayes Hilbert spaces to σ -finite reference measures, allowing for $B^2(\mathbb{R}, \mathfrak{B}_{\mathbb{R}}, \lambda)$. Moreover, Bayes Hilbert spaces include only (μ -a.e.) positive densities. While in the continuous case, values of zero can in many cases be avoided using a suitable density estimation method, they are often replaced with small values in the discrete case (see Pawlowsky-Glahn et al., 2015). In contrast, the square root velocity transformation (Srivastava et al., 2007) allows density values of zero and may be an alternative in such cases, at the price of loosing the Hilbert space structure for the untransformed densities.

Finally, while in practice densities are sometimes directly reported, one often does not observe the response densities directly, but has to first estimate them from individual data to enable the use of density-on-scalar regression. This causes two problems. First, when treating estimated densities as observed, like also in other approaches such as Petersen and Müller (2019) and Han et al. (2020), estimation uncertainty is not accounted for in the analysis. Second, the number of individual observations for each covariate value combination which is available for density estimation can limit the number of covariates that can be included in the model. In the future, we thus aim to extend our approach to also model conditional densities for individual observations, still allowing flexibility in the covariate effects, but with-

out restrictive assumptions such as a particular distribution family as in GAMLSS (Rigby and Stasinopoulos, 2005).

References

- Aitchison, J. (1986). *The Statistical Analysis of Compositional Data*. London, UK, UK: Chapman & Hall, Ltd.
- Beblo, M. and Görges, L. (2018). On the nature of nurture. The malleability of gender differences in work preferences. *Journal of Economic Behavior & Organization* **151**, 19–41.
- Bertrand, M., Kamenica, E., and Pan, J. (2015). Gender Identity and Relative Income within Households. *The Quarterly Journal of Economics* **130**, 571–614.
- Black, S. E. and Spitz-Oener, A. (2010). Explaining women’s success: technological change and the skill content of women’s work. *The Review of Economics and Statistics* **92**, 187–194.
- Boogaart, K. G. van den, Egozcue, J. J., and Pawlowsky-Glahn, V. (2010). Bayes linear spaces. *SORT: statistics and operations research transactions* **34**, 201–222.
- (2014). Bayes Hilbert Spaces. *Australian & New Zealand Journal of Statistics* **56**, 171–194.
- Boogaart, K. G. van den, Tolosana-Delgado, R., and Templ, M. (2015). Regression with compositional response having unobserved components or below detection limit values. *Statistical Modelling* **15**, 191–213.
- Brockhaus, S. and Rügamer, D. (2018). *FDboost: Boosting Functional Regression Models*. R package version 0.3-2.
- Brockhaus, S., Rügamer, D., and Greven, S. (2020). Boosting Functional Regression Models with FDboost. *Journal of Statistical Software* **94**, 1–50.
- Brockhaus, S., Scheipl, F., Hothorn, T., and Greven, S. (2015). The functional linear array model. *Statistical Modelling* **15**, 279–300.
- Bühlmann, P. and Yu, B. (2003). Boosting with the L2 loss: regression and classification. *Journal of the American Statistical Association* **98**, 324–339.
- Chen, S. X. (1999). Beta kernel estimators for density functions. *Computational Statistics & Data Analysis* **31**, 131–145.
- Chernozhukov, V., Fernández-Val, I., and Galichon, A. (2010). Quantile and probability curves without crossing. *Econometrica* **78**, 1093–1125.
- Chernozhukov, V., Fernández-Val, I., and Melly, B. (2013). Inference on counterfactual distributions. *Econometrica* **81**, 2205–2268.
- Cortes, P. and Pan, J. (2018). Occupation and gender. *The Oxford handbook of women and the economy*, 425–452.
- Egozcue, J. J., Díaz-Barrero, J. L., and Pawlowsky-Glahn, V. (2006). Hilbert Space of Probability Density Functions Based on Aitchison Geometry. *Acta Mathematica Sinica* **22**, 1175–1182.
- Fitzenberger, B., Sommerfeld, K., and Steffes, S. (2013). Causal effects on employment after first birth—A dynamic treatment approach. *Labour Economics* **25**, 49–62.

- Han, K., Müller, H.-G., and Park, B. U. (2020). Additive functional regression for densities as responses. *Journal of the American Statistical Association* **115**, 997–1010.
- Happ, C., Scheipl, F., Gabriel, A., and Greven, S. (2019). A general framework for multivariate functional principal component analysis of amplitude and phase variation. *Stat* **8**, e220.
- Hofner, B., Hothorn, T., Kneib, T., and Schmid, M. (2011). A framework for unbiased model selection based on boosting. *Journal of Computational and Graphical Statistics* **20**, 956–971.
- Hothorn, T., Kneib, T., and Bühlmann, P. (2014). Conditional transformation models. *Journal of the Royal Statistical Society: Series B (Statistical Methodology)* **76**, 3–27.
- Hsing, T. and Eubank, R. (2015). *Theoretical Foundations of Functional Data Analysis, with an Introduction to Linear Operators*. Wiley Series in Probability and Statistics. Chichester: John Wiley & Sons, Ltd.
- Kleven, H., Landais, C., Posch, J., Steinhauer, A., and Zweimüller, J. (2019). Child penalties across countries: Evidence and explanations. *AEA Papers and Proceedings*. Vol. 109, 122–26.
- Koenker, R. (2005). *Quantile Regression*. Econometric Society Monographs. Cambridge University Press.
- Kuehnle, D., Oberfichtner, M., and Ostermann, K. (2021). Revisiting Gender Identity and Relative Income within Households: A Cautionary Tale on the Potential Pitfalls of Density Estimators. *Journal of Applied Econometrics*, to appear.
- Li, R., Reich, B. J., and Bondell, H. D. (2021). Deep distribution regression. *Computational Statistics & Data Analysis* **159**, 107203.
- Lutz, R. W. and Bühlmann, P. (2006). Boosting for high-multivariate responses in high-dimensional linear regression. *Statistica Sinica*, 471–494.
- MacEachern, S. N. (1999). Dependent nonparametric processes. *ASA proceedings of the section on Bayesian statistical science*. Vol. 1. Alexandria, Virginia. Virginia: American Statistical Association; 1999, 50–55.
- Ollivier, Y., Pajot, H., and Villani, C. (2014). *Optimal Transport: Theory and Applications*. Vol. 413. Cambridge University Press.
- Park, J. Y. and Qian, J. (2012). Functional regression of continuous state distributions. *Journal of Econometrics* **167**, 397–412.
- Pawlowsky-Glahn, V., Egozcue, J. J., and Tolosana-Delgado, R. (2015). *Modeling and analysis of compositional data*. John Wiley & Sons.
- Petersen, A. and Müller, H.-G. (2019). Fréchet regression for random objects with Euclidean predictors. *The Annals of Statistics* **47**, 691–719.
- Ramsay, J. and Silverman, B. W. (2005). *Functional Data Analysis*. Springer-Verlag New York.
- Rigby, R. A. and Stasinopoulos, D. M. (2005). Generalized additive models for location, scale and shape. *Journal of the Royal Statistical Society: Series C (Applied Statistics)* **54**, 507–554.
- Rügamer, D. and Greven, S. (2020). Inference for L2-Boosting. *Statistics and Computing* **30**, 279–289.

- Sprengholz, M., Wieber, A., and Holst, E. (2020). Gender identity and wives' labor market outcomes in West and East Germany between 1983 and 2016. *Socio-Economic Review*, to appear.
- Srivastava, A., Jermyn, I., and Joshi, S. (2007). Riemannian Analysis of Probability Density Functions with Applications in Vision. *2007 IEEE Conference on Computer Vision and Pattern Recognition*, 1–8.
- Stöcker, A., Brockhaus, S., Schaffer, S., Bronk, B. von, Opitz, M., and Greven, S. (2021). Boosting Functional Response Models for Location, Scale and Shape with an Application to Bacterial Competition. *Statistical Modelling*, to appear.
- Takeuchi, I., Le, Q. V., Sears, T. D., and Smola, A. J. (2006). Nonparametric quantile estimation. *Journal of machine learning research* **7**, 1231–1264.
- Talská, R., Menafoglio, A., Machalová, J., Hron, K., and Fišerová, E. (2018). Compositional regression with functional response. *Computational Statistics & Data Analysis* **123**, 66–85.
- Wood, S. N. (2017). *Generalized Additive Models: An Introduction with R*. 2nd ed. Boca Raton: Chapman and Hall/CRC.
- Yang, H., Baladandayuthapani, V., Rao, A. U. K., and Morris, J. S. (2018). Regression Analyses of Distributions using Quantile Functional Regression. *arXiv preprint arXiv:1810.03496*.

APPENDIX

A Proofs

A.1 Proofs related to Section 2

Proof of Theorem 2.1. This theorem equals Boogaart et al. (2010, Theorem 5), where a brief proof is provided in the appendix. We give an alternative proof showing first that $\mathcal{M}(\mu)$ is a vector space with perturbation and powering analogously defined. For this purpose, let $\nu_1, \nu_2 \in \mathcal{M}(\mu)$ be measures and let $\alpha \in \mathbb{R}$ be a scalar. The vector space axioms, i.e., $\mathcal{M}(\mu)$ is an Abelian group with respect to \oplus , distributivity of \oplus and \odot , associativity of \odot , and $1 \odot \nu = \nu$ for all $\nu \in \mathcal{M}(\mu)$, are straightforward calculations. Thus, we content ourselves with showing that $\nu_1 \oplus \nu_2, \alpha \odot \nu \in \mathcal{M}(\mu)$, which requires some more work. To see this, two properties have to be verified: the resulting measures have to be σ -finite and have the same null sets as μ . The former is shown in the proof of Theorem 4 in appendix A of Boogaart et al., 2010. To show that both $\nu_1 \oplus \nu_2$ and $\alpha \odot \nu$ have the same null sets as μ , we first show that for every $A \in \mathcal{A}$ and every $f : \mathcal{T} \rightarrow \mathbb{R}_0^+$, the implication

$$\left(f > 0 \wedge \int_A f \, d\mu = 0 \right) \Rightarrow \mu(A) = 0 \quad (\text{A.1})$$

is true. Let f be a function that fulfills the properties on the left side of the implication and let $A \in \mathcal{A}$. For the sets $A_0 := \{f \geq 1\} \cap A$ and $A_n := \{\frac{1}{n+1} \leq f < \frac{1}{n}\} \cap A$, we get $A = \bigsqcup_{n \in \mathbb{N}_0} A_n$. Moreover, for every $n \in \mathbb{N}_0$, we have

$$\int_{A_n} f \, d\mu \geq \int_{A_n} \frac{1}{n+1} \, d\mu = \frac{1}{n+1} \mu(A_n). \quad (\text{A.2})$$

Now, assume that $\mu(A) \neq 0$, i.e., $\mu(A) > 0$. Then, there exists an $m \in \mathbb{N}_0$ such that $\mu(A_m) > 0$, because $\mu(A) = \sum_{n \in \mathbb{N}_0} \mu(A_n)$. Thus, the inequality

$$\int_A f \, d\mu \geq \int_{A_m} f \, d\mu \stackrel{(\text{A.2})}{\geq} \frac{1}{m+1} \mu(A_m) > 0$$

holds. This is a contradiction to the hypothesis that $\int_A f = 0$, which proves implication (A.1).

Thereby, it is easy to show that $\nu_1 \oplus \nu_2$ and $\alpha \odot \nu$ have the same null sets as μ : Let $A \in \mathcal{A}$ such that $0 = (\nu_1 \oplus \nu_2)(A) = \int_A f_{\nu_1} f_{\nu_2} \, d\mu$. We have $f_{\nu_1} f_{\nu_2} > 0$. Using Equation (A.1), we immediately get $\mu(A) = 0$. Analogously, we have $(f_\nu)^\alpha > 0$ for every $\alpha \in \mathbb{R}$. With Equation (A.1) it follows $\mu(A) = 0$, if $(\alpha \odot \nu)(A) = 0$ for all $A \in \mathcal{A}$. The converse implications are trivial in both cases. This proves that $\nu_1 \oplus \nu_2, \alpha \odot \nu \in \mathcal{M}(\mu)$ and thus, $\mathcal{M}(\mu)$ is a real vector space with operations \oplus and \odot .

It remains to prove that also $\mathcal{B}(\mu)$ is a real vector space. One easily shows that the set $[\mu]$ is a vector subspace of $\mathcal{M}(\mu)$. Furthermore, the relation $=_{\mathcal{B}}$ defines an equivalence relation on $\mathcal{M}(\mu)$ satisfying $\nu_1 \ominus \nu_2 \in [\mu]$ if and only if $\nu_1 =_{\mathcal{B}} \nu_2$ for $\nu_1, \nu_2 \in \mathcal{M}(\mu)$. By elementary linear algebra it follows that $\mathcal{B}(\mu) = \mathcal{M}(\mu)/[\mu]$ is a vector space with respect to the evident quotient operations \oplus and \odot . \square

Proof of Proposition 2.2. This proposition is proven in Boogaart et al. (2014, Propositions 2, 4 and 5) in the case $p = 1$. We show the statements for arbitrary $1 \leq p < \infty$, because we need them in particular for $p = 2$.

Let $1 \leq p < \infty$ and let $\nu \in B^p(\mu)$ be a measure. The integral $\int_{\mathcal{T}} \log f_{\nu} d\mu$ exists because of $\log f_{\nu} \in L^p(\mu)$. Furthermore, it is straightforward to show that for every $\nu_2 \in B^p(\mu)$ with $\nu_2 =_{\mathcal{B}} \nu$ the clr images are equal, $\text{clr}[\nu] = \text{clr}[\nu_2]$. Hence, the clr image of $[\nu]$ is well-defined on $B^p(\mu)$. Next, we show that $\text{clr}[\nu] \in L_0^p(\mu)$, which is the case if $\text{clr}[\nu] \in L^p(\mu)$ and $\int_{\mathcal{T}} \text{clr}[\nu] d\mu = 0$. The first statement corresponds to $\int_{\mathcal{T}} |\text{clr}[\nu]|^p d\mu < \infty$, which is equivalent to $\|\text{clr}[\nu]\|_{L^p(\mu)} < \infty$. Using the Minkowski inequality, we get

$$\|\text{clr}[\nu]\|_{L^p(\mu)} = \|\log f_{\nu} - \mathcal{S}(f_{\nu})\|_{L^p(\mu)} \leq \|\log f_{\nu}\|_{L^p(\mu)} + \|\mathcal{S}(f_{\nu})\|_{L^p(\mu)}.$$

As $\nu \in B^p(\mu)$, we have $\log f_{\nu} \in L^p(\mu)$ and therefore the first term is finite. For the second term, the function in the norm is a constant, thus it is an element of $L^p(\mu)$ since μ is finite. Together, we get $\|\text{clr}[\nu]\|_{L^p(\mu)} < \infty$. Moreover,

$$\int_{\mathcal{T}} \text{clr}[\nu] d\mu = \int_{\mathcal{T}} \log f_{\nu} - \mathcal{S}(f_{\nu}) d\mu = \mu(\mathcal{T}) \mathcal{S}(f_{\nu}) - \mu(\mathcal{T}) \mathcal{S}(f_{\nu}) = 0.$$

Hence, it follows that $\text{clr}[\nu] \in L_0^p(\mu)$. Furthermore, the clr transformation is linear:

$$\begin{aligned} \text{clr}[\alpha \odot f_{\nu} \oplus f_{\nu_2}] &= \log((f_{\nu})^{\alpha} f_{\nu_2}) - \mathcal{S}((f_{\nu})^{\alpha} f_{\nu_2}) \\ &= \alpha (\log f_{\nu} - \mathcal{S}(f_{\nu})) + \log f_{\nu_2} - \mathcal{S}(f_{\nu_2}) = \alpha \text{clr}[f_{\nu}] + \text{clr}[f_{\nu_2}]. \end{aligned}$$

It remains to show that it is bijective. For $\tilde{f} \in L_0^p(\mu)$, we have

$$\text{clr}[\exp \tilde{f}] = \log(\exp \tilde{f}) - \mathcal{S}(\exp \tilde{f}) = \tilde{f} - \frac{1}{\mu(\mathcal{T})} \int_{\mathcal{T}} \tilde{f} d\mu = \tilde{f},$$

using that the last integral is zero since $\tilde{f} \in L_0^p(\mu)$. Conversely, for $f \in B^p(\mu)$, we get

$$\exp(\text{clr}[f]) = \exp(\log f - \mathcal{S}(f)) = \frac{f}{\exp(\mathcal{S}(f))} = f$$

and therefore, the clr transformation is bijective. \square

Proposition A.1. *The inner product on $B^2(\mu)$ is an inner product.*

Proof. Linearity of $\langle \cdot, \cdot \rangle_{B^2(\mu)}$ follows from the linearity of the clr transformation, see Proposition 2.2, and basic calculation rules. Symmetry is obvious by the commutativity of multiplication in \mathbb{R} . It remains to show that $\langle \cdot, \cdot \rangle_{B^2(\mu)}$ is positive definite. For this purpose, let $f_{\nu} \in B^2(\mu)$ be a density.

- We have $\langle f_{\nu}, f_{\nu} \rangle_{B^2(\mu)} = \int_{\mathcal{T}} (\text{clr}[f_{\nu}])^2 d\mu \geq 0$ because the integrand is nonnegative.
- We need to show that $\langle f_{\nu}, f_{\nu} \rangle_{B^2(\mu)} = 0 \iff f_{\nu} = 0$.

“ \Rightarrow ” If $\langle f_\nu, f_\nu \rangle_{B^2(\mu)} = \int_{\mathcal{T}} (\text{clr}[f_\nu])^2 d\mu = 0$, then $\text{clr}[f_\nu] = 0$ must hold. This is equivalent to $\log f_\nu = \mathcal{S}(f_\nu)$ μ -almost everywhere, which means $\log f_\nu$ is a constant function. Then, f_ν is constant as well and thus $f_\nu = 0$.

“ \Leftarrow ” If otherwise $f_\nu = 0$, then $\text{clr}[f_\nu] = 0$ by linearity of the clr transformation, see Proposition 2.2, and therefore $\langle f_\nu, f_\nu \rangle_{B^2(\mu)} = 0$. \square

Proof of Theorem 2.3. We provide an alternative proof to Boogaart et al. (2014): It is a known fact from functional analysis that $L^2(\mu)$ is a Hilbert space. As a closed subspace, $L_0^2(\mu)$ is a Hilbert space as well. As the clr transformation $\text{clr} : B^2(\mu) \rightarrow L_0^2(\mu)$ is isometric, it follows that also $B^2(\mu)$ is a Hilbert space. \square

Note that under very modest assumptions on the measure space $(\mathcal{T}, \mathcal{A}, \mu)$, the Hilbert spaces $L^2(\mu)$ and $L_0^2(\mu)$ are separable, see Elstrodt (2011, Korollar 2.29). This was used in the pioneering work of Egozcue et al. (2006) to construct the Bayes Hilbert space and show its separability.

Proposition A.2. *For any $\mathcal{T}_0 \in \mathcal{A}$, the Bayes Hilbert space $B^2(\mathcal{T}_0) = B^2(\mathcal{T}_0, \mathcal{A} \cap \mathcal{T}_0, \mu)$ is a closed subspace of $B^2(\mathcal{T}) = B^2(\mathcal{T}, \mathcal{A}, \mu)$ with respect to the embedding*

$$\iota : B^2(\mathcal{T}_0) \hookrightarrow B^2(\mathcal{T}), \quad \tilde{f} \mapsto \begin{cases} \tilde{f} & \text{on } \mathcal{T}_0 \\ \exp \mathcal{S}_{\mathcal{T}_0}(\tilde{f}) & \text{on } \mathcal{T} \setminus \mathcal{T}_0 \end{cases},$$

where $\exp \mathcal{S}_{\mathcal{T}_0}(\tilde{f})$ is the geometric mean of \tilde{f} on \mathcal{T}_0 , see Section 3.3. This means that ι is linear and preserves the norm. The orthogonal projection is given by

$$P : B^2(\mathcal{T}) \rightarrow B^2(\mathcal{T}), \quad f \mapsto \iota(f|_{\mathcal{T}_0}),$$

where $f|_{\mathcal{T}_0} \in B^2(\mathcal{T}_0)$ denotes the function f restricted to \mathcal{T}_0 . In particular, this means,

$$(a) \quad P^2 = P,$$

$$(b) \quad \|P\| := \sup_{f \neq 0} \frac{\|P(f)\|_{B^2(\mathcal{T})}}{\|f\|_{B^2(\mathcal{T})}} = 1,$$

$$(c) \quad P^* = P.$$

Proof. It is straightforward to show that ι is well-defined and linear. Let $\tilde{f} \in B^2(\mathcal{T}_0)$ and $g \in B^2(\mathcal{T})$. Preservation of the norm is implied by the more general preservation of the inner product, $\langle \iota(\tilde{f}), g \rangle_{B^2(\mathcal{T})} = \langle \tilde{f}, g|_{\mathcal{T}_0} \rangle_{B^2(\mathcal{T}_0)}$, considering the special case $g = \iota(\tilde{f})$. As we need the preservation of the inner product later, we show this more general property instead of just preservation of the norm. We have

$$\langle \iota(\tilde{f}), g \rangle_{B^2(\mathcal{T})} = \int_{\mathcal{T}} \text{clr}[\iota(\tilde{f})] \left((\log g - \mathcal{S}_{\mathcal{T}_0}(g|_{\mathcal{T}_0})) + (\mathcal{S}_{\mathcal{T}_0}(g|_{\mathcal{T}_0}) - \mathcal{S}_{\mathcal{T}}(g)) \right) d\mu,$$

where the last term $\mathcal{S}_{\mathcal{T}_0}(g|_{\mathcal{T}_0}) - \mathcal{S}_{\mathcal{T}}(g)$ is constant. Thus, it does not contribute to the integral as $\text{clr}[\iota(\tilde{f})] \in L_0^2(\mathcal{T})$. By the additivity of μ we get

$$\mathcal{S}_{\mathcal{T}}(\iota(\tilde{f})) = \frac{1}{\mu(\mathcal{T})} \left(\int_{\mathcal{T}_0} \log \tilde{f} d\mu + \int_{\mathcal{T} \setminus \mathcal{T}_0} \mathcal{S}_{\mathcal{T}_0}(\tilde{f}) d\mu \right) = \mathcal{S}_{\mathcal{T}_0}(\tilde{f}) \quad (\text{A.3})$$

and thus

$$\langle \iota(\tilde{f}), g \rangle_{B^2(\mathcal{T})} = \int_{\mathcal{T}} \left(\log \iota(\tilde{f}) - \mathcal{S}_{\mathcal{T}_0}(\tilde{f}) \right) (\log g - \mathcal{S}_{\mathcal{T}_0}(g|_{\mathcal{T}_0})) \, d\mu.$$

Note that the first factor of the integrand is zero on $\mathcal{T} \setminus \mathcal{T}_0$ as $\iota(\tilde{f}) = \exp \mathcal{S}_{\mathcal{T}_0}(\tilde{f})$ on this set. This leaves us with

$$\langle \iota(\tilde{f}), g \rangle_{B^2(\mathcal{T})} = \int_{\mathcal{T}_0} \text{clr}_{\mathcal{T}_0} [\tilde{f}] \, \text{clr}_{\mathcal{T}_0} [g|_{\mathcal{T}_0}] \, d\mu = \langle \tilde{f}, g|_{\mathcal{T}_0} \rangle_{B^2(\mathcal{T}_0)}, \quad (\text{A.4})$$

i.e., ι preserves the inner product. In particular, ι preserves the norm and is an embedding. Being a Hilbert space, $B^2(\mathcal{T}_0)$ is complete and thus is a closed subspace of $B^2(\mathcal{T})$. Now, we show that

$$P : B^2(\mathcal{T}) \rightarrow B^2(\mathcal{T}), \quad f \mapsto \iota(f|_{\mathcal{T}_0}),$$

is an orthogonal projection.

(a) On \mathcal{T}_0 , the embedding ι is the identity and thus $P(P(f)) = P(f)$ holds.

(b) Let $f \in B^2(\mathcal{T})$. First, we show $\|P(f)\|_{B^2(\mathcal{T})}^2 \leq \|f\|_{B^2(\mathcal{T})}^2$. We have

$$\|f\|_{B^2(\mathcal{T})}^2 = \int_{\mathcal{T}_0} \left(\text{clr}_{\mathcal{T}_0}[f] + (\mathcal{S}_{\mathcal{T}_0}(f) - \mathcal{S}_{\mathcal{T}}(f)) \right)^2 \, d\mu + \int_{\mathcal{T} \setminus \mathcal{T}_0} (\text{clr}_{\mathcal{T}}[f])^2 \, d\mu.$$

The first term is bounded from below by $\|f|_{\mathcal{T}_0}\|_{B^2(\mathcal{T}_0)}^2$ since $\text{clr}_{\mathcal{T}_0}[f]$ is orthogonal to the constant $\mathcal{S}_{\mathcal{T}_0}(f) - \mathcal{S}_{\mathcal{T}}(f)$ and the square integral of the latter is nonnegative. Furthermore, the last term is nonnegative, i.e., $\|f\|_{B^2(\mathcal{T})}^2 \geq \|f|_{\mathcal{T}_0}\|_{B^2(\mathcal{T}_0)}^2$. As ι preserves the norm, this implies the claim. Since $P(f) \in B^2(\mathcal{T})$ saturates the inequality because of (a) we get $\|P\| = 1$.

(c) Let $f, g \in B^2(\mathcal{T})$. Then, using the symmetry of the inner product, we have

$$\langle P(f), g \rangle_{B^2(\mathcal{T})} \stackrel{(\text{A.4})}{=} \langle f|_{\mathcal{T}_0}, g|_{\mathcal{T}_0} \rangle_{B^2(\mathcal{T}_0)} \stackrel{(\text{A.4})}{=} \langle f, P(g) \rangle_{B^2(\mathcal{T})}. \quad \square$$

A.2 Proofs related to Section 3

Proof of Equation (3.5). This proof requires knowledge about differential calculus for real functionals. A review can be found in Badiale and Serra (2011, Section 1.3). We want to show that the negative gradient of the loss functional

$$\rho_{y_i} : B^2(\mu) \rightarrow \mathbb{R}, \quad f_{\nu_1} \mapsto \|y_i \ominus f_{\nu_1}\|_{B^2(\mu)}^2$$

at $f_{\nu_1} \in B^2(\mu)$ for $y_i \in B^2(\mu)$ exists and determine it. First, we show that ρ_{y_i} is Fréchet differentiable at $f_{\nu_1} \in B^2(\mu)$, i.e., that there exists $A \in (B^2(\mu))'$ such that

$$\lim_{\|f_{\nu_2}\|_{B^2(\mu)} \rightarrow 0} \frac{\rho_{y_i}(f_{\nu_1} \oplus f_{\nu_2}) - \rho_{y_i}(f_{\nu_1}) - A(f_{\nu_2})}{\|f_{\nu_2}\|_{B^2(\mu)}} = 0, \quad (\text{A.5})$$

where $(B^2(\mu))' := \{A : B^2(\mu) \rightarrow \mathbb{R} \mid A \text{ linear and continuous}\}$ is the topological dual of $B^2(\mu)$. Consider $A = A_{y_i, f_{\nu_1}} : B^2(\mu) \rightarrow \mathbb{R}, f_{\nu_2} \mapsto \langle \ominus 2 \odot (y_i \ominus f_{\nu_1}), f_{\nu_2} \rangle_{B^2(\mu)}$. Then $A \in (B^2(\mu))'$ and for $f_{\nu_1}, f_{\nu_2} \in B^2(\mu)$, we have

$$\begin{aligned} \rho_{y_i}(f_{\nu_1} \oplus f_{\nu_2}) - \rho_{y_i}(f_{\nu_1}) - A(f_{\nu_2}) &= \|y_i \ominus (f_{\nu_1} \oplus f_{\nu_2})\|_{B^2(\mu)}^2 - \|y_i \ominus f_{\nu_1}\|_{B^2(\mu)}^2 \\ &\quad - \langle \ominus 2 \odot (y_i \ominus f_{\nu_1}), f_{\nu_2} \rangle_{B^2(\mu)} \\ &= \|y_i \ominus f_{\nu_1}\|_{B^2(\mu)}^2 - 2\langle y_i \ominus f_{\nu_1}, f_{\nu_2} \rangle_{B^2(\mu)} + \|f_{\nu_2}\|_{B^2(\mu)}^2 \\ &\quad - \|y_i \ominus f_{\nu_1}\|_{B^2(\mu)}^2 + 2\langle y_i \ominus f_{\nu_1}, f_{\nu_2} \rangle_{B^2(\mu)} \\ &= \|f_{\nu_2}\|_{B^2(\mu)}^2. \end{aligned}$$

This implies that the limit in (A.5) is zero. Thus, ρ_{y_i} is Fréchet differentiable at $f_{\nu_1} \in B^2(\mu)$ with differential $d\rho_{y_i}(f_{\nu_1}) = A = A_{y_i, f_{\nu_1}}$. As $B^2(\mu)$ is a Hilbert space, Riesz' Representation Theorem holds and the gradient of ρ_{y_i} at f_{ν_1} is $\nabla \rho_{y_i}(f_{\nu_1}) = \ominus 2 \odot (y_i \ominus f_{\nu_1})$. \square

Proposition A.3. *Consider the mixed case, i.e., $B^2(\mu) = B^2(I, \mathfrak{B}, \mu)$ with $\mu = \delta + \lambda$, where $\delta = \sum_{d=1}^D w_d \delta_{t_d}$ with $\{t_1, \dots, t_D\} = \mathcal{D} \subset I$ and $w_d > 0$. For $\mathcal{C} := I \setminus \mathcal{D}$, the orthogonal complement of the Bayes Hilbert space $B^2(\lambda) = B^2(\mathcal{C}, \mathfrak{B} \cap \mathcal{C}, \lambda)$ in $B^2(\mu)$ is $B^2(\delta^\bullet) = B^2(\mathcal{D}^\bullet, \mathcal{P}(\mathcal{D}^\bullet), \delta^\bullet)$, where $\mathcal{D}^\bullet := \mathcal{D} \cup \{t_{D+1}\}$ with $t_{D+1} \in \mathbb{R} \setminus \mathcal{D}$ and $\delta^\bullet := \sum_{d=1}^{D+1} w_d \delta_{t_d}$, $w_{D+1} := \lambda(I)$. The embeddings to consider $B^2(\lambda)$ and $B^2(\delta^\bullet)$ as subspaces of $B^2(\mu)$ are*

$$\begin{aligned} \iota_c : B^2(\lambda) &\hookrightarrow B^2(\mu) & f_c &\mapsto \begin{cases} f_c & \text{on } \mathcal{C} \\ \exp \mathcal{S}_\lambda(f_c) & \text{on } \mathcal{D} \end{cases} \\ \iota_d : B^2(\delta^\bullet) &\hookrightarrow B^2(\mu) & f_d &\mapsto \begin{cases} f_d(t_{D+1}) & \text{on } \mathcal{C} \\ f_d & \text{on } \mathcal{D} \end{cases}, \end{aligned}$$

where $\exp \mathcal{S}_\lambda(f_c)$ is the geometric mean of f_c , , see Section 3.3. This means, for every $\alpha \in \mathbb{R}$, $f_c, g_c \in B^2(\lambda)$, $f_d, g_d \in B^2(\delta^\bullet)$:

- (a) $\iota_c(\alpha \odot f_c \oplus g_c) = \alpha \odot \iota_c(f_c) \oplus \iota_c(g_c)$ and $\iota_d(\alpha \odot f_d \oplus g_d) = \alpha \odot \iota_d(f_d) \oplus \iota_d(g_d)$ (Linearity),
- (b) $\|\iota_c(f_c)\|_{B^2(\mu)} = \|f_c\|_{B^2(\lambda)}$ and $\|\iota_d(f_d)\|_{B^2(\mu)} = \|f_d\|_{B^2(\delta^\bullet)}$ (Preservation of the norm),
- (c) $\langle \iota_c(f_c), \iota_d(f_d) \rangle_{B^2(\mu)} = 0$ (Orthogonality).
- (d) For every $f \in B^2(\mu)$, there exist unique functions $f_c \in B^2(\lambda)$, $f_d \in B^2(\delta^\bullet)$ such that $f = \iota_c(f_c) \oplus \iota_d(f_d)$, given by

$$f_c : \mathcal{C} \rightarrow \mathbb{R}, \quad t \mapsto f(t), \quad f_d : \mathcal{D}^\bullet \rightarrow \mathbb{R}, \quad t \mapsto \begin{cases} 1, & t = t_{D+1} \\ \frac{f(t)}{\exp \mathcal{S}_\lambda(f)}, & t \in \mathcal{D}. \end{cases} \quad (\text{A.6})$$

Proof. We have $B^2(\lambda) = B^2(\mathcal{C}, \mathfrak{B} \cap \mathcal{C}, \lambda) = B^2(\mathcal{C}, \mathfrak{B} \cap \mathcal{C}, \mu)$, per definition of μ . Since $\mathcal{C} \in \mathfrak{B}$, we obtain from Proposition A.2 that ι_c is well-defined and fulfills (a) and (b). For ι_d , well-definedness is obvious.

(a) For ι_d , this is straightforward by definition.

(b) Let $f_d \in B^2(\delta^\bullet)$. With $\mu(I) = \delta(\mathcal{D}) + \lambda(I) = \delta^\bullet(\mathcal{D}^\bullet)$ we have

$$\mathcal{S}_\mu(\iota_d(f_d)) = \frac{1}{\mu(I)} \left(\int_{\mathcal{D}} \log f_d(t_d) d\delta + \lambda(I) \log f_d(t_{D+1}) \right) = \mathcal{S}_{\delta^\bullet}(f_d). \quad (\text{A.7})$$

This yields

$$\begin{aligned} \|\iota_d(f_d)\|_{B^2(\mu)}^2 &= \int_{\mathcal{D}} (\log f_d - \mathcal{S}_{\delta^\bullet}(f_d))^2 d\delta + \lambda(I) (\log f_d(t_{D+1}) - \mathcal{S}_{\delta^\bullet}(f_d))^2 \\ &= \int_{\mathcal{D}^\bullet} (\log f_d - \mathcal{S}_{\delta^\bullet}(f_d))^2 d\delta^\bullet = \|f_d\|_{B^2(\delta^\bullet)}^2. \end{aligned}$$

(c) For $f_c \in B^2(\lambda)$, $f_d \in B^2(\delta^\bullet)$, we have

$$\langle \iota_c(f_c), \iota_d(f_d) \rangle_{B^2(\mu)} \stackrel{(\text{A.4})}{=} \langle f_c, \iota_d(f_d)|_{\mathcal{C}} \rangle_{B^2(\lambda)} = 0,$$

as $\iota_d(f_d)|_{\mathcal{C}}$ is a constant and thus $0 \in B^2(\lambda)$.

(d) For $f \in B^2(\mu)$ consider f_c and f_d as in (A.6). With $f \in B^2(\mu)$, we have $\int_{\mathcal{D}} (\log f)^2 d\delta + \int_I (\log f)^2 d\lambda = \int_I (\log f)^2 d\mu < \infty$, thus all terms on the left side have to be finite, as well. Looking at the second term, we get $f_c \in B^2(\lambda)$ since the Lebesgue integral yields the same results on I and \mathcal{C} . Moreover, $f_c \in B^2(\lambda) \subset B^1(\lambda)$ implies $\mathcal{S}_\lambda(f) = \mathcal{S}_\lambda(f_c) < \infty$. Similarly, from $\int_{\mathcal{D}} (\log f)^2 d\delta < \infty$ it follows $\mathcal{S}_\delta(f) < \infty$. Then, we get

$$\begin{aligned} \int_{\mathcal{D}^\bullet} (\log f_d)^2 d\delta^\bullet &= \int_{\mathcal{D}} (\log f - \mathcal{S}_\lambda(f))^2 d\delta + \lambda(I) \\ &= \int_{\mathcal{D}} (\log f)^2 d\delta - 2\delta(\mathcal{D})\mathcal{S}_\delta(f)\mathcal{S}_\lambda(f) + \delta(\mathcal{D})\mathcal{S}_\lambda(f)^2 + \lambda(I) < \infty, \end{aligned}$$

i.e., $f_d \in B^2(\delta^\bullet)$. Finally,

$$\iota_c(f_c) \oplus \iota_d(f_d) = \left\{ \begin{array}{ll} f & \text{on } \mathcal{C} \\ \exp(\mathcal{S}_\lambda(f)) \frac{f}{\exp(\mathcal{S}_\lambda(f))} & \text{on } \mathcal{D} \end{array} \right\} = f.$$

As we already showed that $B^2(\lambda)$ and $B^2(\delta^\bullet)$ form an orthogonal decomposition of $B^2(\mu)$ in (a) – (c), the representation of f by f_c and f_d is unique and thus $B^2(\delta^\bullet)$ is the orthogonal complement of $B^2(\lambda)$ in $B^2(\mu)$. \square

Proposition A.4. *The orthogonal complement of $L_0^2(\lambda) = L_0^2(\mathcal{C}, \mathfrak{B}, \lambda)$ in $L_0^2(\mu) = L_0^2(I, \mathfrak{B}, \mu)$ is $L_0^2(\delta^\bullet) = L_0^2(\mathcal{D}^\bullet, \mathcal{P}(\mathcal{D}^\bullet), \delta^\bullet)$ with respect to the embeddings*

$$\begin{aligned} \tilde{\iota}_c : L_0^2(\lambda) &\hookrightarrow L_0^2(\mu) & \tilde{f}_c &\mapsto \begin{cases} \tilde{f}_c & \text{on } \mathcal{C} \\ 0 & \text{on } \mathcal{D} \end{cases} \\ \tilde{\iota}_d : L_0^2(\delta^\bullet) &\hookrightarrow L_0^2(\mu) & \tilde{f}_d &\mapsto \begin{cases} \tilde{f}_d(t_{D+1}) & \text{on } \mathcal{C} \\ \tilde{f}_d & \text{on } \mathcal{D} \end{cases}, \end{aligned}$$

with all measures and sets defined as in Proposition A.3. The decomposition is equivalent to the one in Proposition A.3, i.e., for all $f_c \in B^2(\lambda)$ and all $f_d \in B^2(\delta^\bullet)$ we have $\tilde{\iota}_c(\text{clr}_\lambda[f_c]) = \text{clr}_\mu[\iota_c(f_c)]$ and $\tilde{\iota}_d(\text{clr}_{\delta^\bullet}[f_d]) = \text{clr}_\mu[\iota_d(f_d)]$. Moreover, the representation of $\tilde{f} \in L_0^2(\mu)$ as $\tilde{f} = \tilde{\iota}_c(\tilde{f}_c) + \tilde{\iota}_d(\tilde{f}_d)$ with unique functions $\tilde{f}_c \in L_0^2(\lambda)$, $\tilde{f}_d \in L_0^2(\delta^\bullet)$ given by

$$\begin{aligned} \tilde{f}_c : \mathcal{C} &\rightarrow \mathbb{R} & t &\mapsto \tilde{f}(t) - \frac{1}{\lambda(\mathcal{C})} \int_{\mathcal{C}} \tilde{f} \, d\lambda, \\ \tilde{f}_d : \mathcal{D}^\bullet &\rightarrow \mathbb{R} & t &\mapsto \begin{cases} \frac{1}{\lambda(\mathcal{C})} \int_{\mathcal{C}} \tilde{f} \, d\lambda & , t = t_{D+1} \\ \tilde{f}(t) & , t \in \mathcal{D} \end{cases}, \end{aligned} \quad (\text{A.8})$$

is equivalent to the unique representation of $f \in B^2(\mu)$ as $f = \iota_c(f_c) \oplus \iota_d(f_d)$, see (A.6), via clr transformations. This means, for $\tilde{f} = \text{clr}_\mu[f] \in L_0^2(\mu)$ we have $\tilde{f}_c = \text{clr}_\lambda[f_c] \in L_0^2(\lambda)$ and $\tilde{f}_d = \text{clr}_{\delta^\bullet}[f_d] \in L_0^2(\delta^\bullet)$.

Proof. Linearity, preservation of the norm, and orthogonality are straightforward calculations. Thus, $L_0^2(\lambda)$ and $L_0^2(\delta^\bullet)$ form an orthogonal decomposition of $L_0^2(\mu)$. To show the equivalence to the decomposition in Proposition A.3, consider $f_c \in B^2(\lambda)$ and $f_d \in B^2(\delta^\bullet)$. Then, we have

$$\begin{aligned} \text{clr}_\mu[\iota_c(f_c)] &= \log \iota_c(f_c) - \mathcal{S}_{B^2(\mathcal{T}, \mathcal{A}, \mu)}(\iota_c(f_c)) \stackrel{(\text{A.3})}{=} \log \iota_c(f_c) - \mathcal{S}_{B^2(\mathcal{C}, \mathfrak{B} \cap \mathcal{C}, \mu)}(f_c) \\ &= \begin{cases} \log f_c - \mathcal{S}_\lambda(f_c) & \text{on } \mathcal{C} \\ \mathcal{S}_\lambda(f_c) - \mathcal{S}_\lambda(f_c) & \text{on } \mathcal{D} \end{cases} = \tilde{\iota}_c(\text{clr}_\lambda[f_c]), \\ \text{clr}_\mu[\iota_d(f_d)] &= \log \iota_d(f_d) - \mathcal{S}_\mu(\iota_d(f_d)) \stackrel{(\text{A.7})}{=} \log \iota_d(f_d) - \mathcal{S}_{\delta^\bullet}(f_d) \\ &= \begin{cases} \log f_d(t_{D+1}) - \mathcal{S}_{\delta^\bullet}(f_d) & \text{on } \mathcal{C} \\ \log f_d - \mathcal{S}_{\delta^\bullet}(f_d) & \text{on } \mathcal{D} \end{cases} = \tilde{\iota}_d(\text{clr}_{\delta^\bullet}[f_d]). \end{aligned}$$

For $\tilde{f} \in L_0^2(\mu)$ consider \tilde{f}_c and \tilde{f}_d as in (A.8). As $\tilde{f} \in L_0^2(\mu)$, we have $\int_{\mathcal{D}} \tilde{f}^2 \, d\delta + \int_I \tilde{f}^2 \, d\lambda = \int_I \tilde{f}^2 \, d\mu < \infty$. Thus, both terms on the left side are finite and in particular, $\tilde{f} \in L^2(\lambda) \subset L^1(\lambda)$. Then,

$$\int_{\mathcal{C}} \tilde{f}_c^2 \, d\lambda = \int_{\mathcal{C}} \left(\tilde{f} - \frac{1}{\lambda(\mathcal{C})} \int_{\mathcal{C}} \tilde{f} \, d\lambda \right)^2 \, d\lambda = \int_{\mathcal{C}} \tilde{f}^2 \, d\lambda - \frac{1}{\lambda(\mathcal{C})} \left(\int_{\mathcal{C}} \tilde{f} \, d\lambda \right)^2 < \infty.$$

It is straightforward to show $\int_{\mathcal{C}} \tilde{f}_c \, d\lambda = 0$, i.e., $\tilde{f}_c \in L_0^2(\lambda)$. Moreover, we have

$$\int_{\mathcal{D}^\bullet} \tilde{f}_d^2 \, d\delta^\bullet = \int_{\mathcal{D}} \tilde{f}^2 \, d\delta + \frac{\lambda(I)}{\lambda(\lambda(I))^2} \left(\int_{\mathcal{C}} \tilde{f} \, d\lambda \right)^2 < \infty.$$

The same calculation without squares shows $\int_{\mathcal{D}^\bullet} \tilde{f}_d \, d\delta^\bullet = \int_{\mathcal{D}} \tilde{f} \, d\delta + \int_{\mathcal{C}} \tilde{f} \, d\lambda = \int_I \tilde{f} \, d\mu$, which is zero as $\tilde{f} \in L_0^2(\mu)$ and thus $\tilde{f}_d \in L_0^2(\delta^\bullet)$. Furthermore,

$$\tilde{\iota}_c(\tilde{f}_c) + \tilde{\iota}_d(\tilde{f}_d) = \begin{cases} \tilde{f} - \frac{1}{\lambda(\mathcal{C})} \int_{\mathcal{C}} \tilde{f} \, d\lambda + \frac{1}{\lambda(\mathcal{C})} \int_{\mathcal{C}} \tilde{f} \, d\lambda & \text{on } \mathcal{C} \\ 0 + \tilde{f} & \text{on } \mathcal{D} \end{cases} = \tilde{f}$$

and the uniqueness of the representation follows from $L_0^2(\lambda)$ and $L_0^2(\delta^\bullet)$ being an orthogonal decomposition of $L_0^2(\mu)$. This implies that $L_0^2(\delta^\bullet)$ is the orthogonal complement of $L_0^2(\lambda)$ in $L_0^2(\mu)$. Finally, we show the equivalence to the representation $f = \iota_c(f_c) \oplus \iota_d(f_d)$ of $f \in B^2(\mu)$ with unique functions $f_c \in B^2(\lambda)$ and $f_d \in B^2(\delta^\bullet)$. Consider $\tilde{f} = \text{clr}_\mu[f] \in L_0^2(\mu)$. With the equivalence of the decompositions and linearity of clr_μ we get

$$\tilde{\iota}_c(\tilde{f}_c) + \tilde{\iota}_d(\tilde{f}_d) = \tilde{f} = \text{clr}_\mu[f] = \text{clr}_\mu[\iota_c(f_c) \oplus \iota_d(f_d)] = \tilde{\iota}_c(\text{clr}_\lambda[f_c]) + \tilde{\iota}_d(\text{clr}_{\delta^\bullet}[f_d])$$

and uniqueness of the representation yields $\tilde{f}_c = \text{clr}_\lambda[f_c]$ and $\tilde{f}_d = \text{clr}_{\delta^\bullet}[f_d]$. \square

Proof of Equation (3.10). Consider $\mathcal{T} = I \subset \mathbb{R}$ and $\mu = \sum_{d=1}^D w_d \delta_{t_d} + \lambda$ for $\mathcal{D} = \{t_1, \dots, t_D\} \subset I$. Let $s \in I$ and $A_n \subseteq I$ be intervals such that A_n is centered at s for all $n \in \mathbb{N}$, $\bigcap_{n \in \mathbb{N}} A_n = \{s\}$ and $A_{n+1} \subset A_n$, for $n \in \mathbb{N}$. It is sufficient to show

$$\lim_{n \rightarrow \infty} \frac{\mathbb{P}_j(A_n)}{\mu(A_n)} = \hat{h}_j(s) \quad (\text{A.9})$$

to prove (3.10).

(a) In the continuous case, i.e., $\mathcal{D} = \emptyset$, we have

$$\lim_{n \rightarrow \infty} \frac{\mathbb{P}_j(A_n)}{\lambda(A_n)} = \lim_{n \rightarrow \infty} \frac{1}{\lambda(A_n)} \int_{A_n} \hat{h}_j d\lambda = \hat{h}_j(s)$$

using Lebesgue's Differentiation Theorem (Wheeden and Zygmund, 2015, Theorem 7.2) in the last equation. Note that the equation holds for all s in the interior of I (not only μ -a.e.), if \hat{h}_j is continuous¹. Extending \hat{h}_j outside of I by 0 also yields the statement for the boundary values of I .

(b) In the mixed case, we have

$$\lim_{n \rightarrow \infty} \frac{\mathbb{P}_j(A_n)}{\mu(A_n)} = \lim_{n \rightarrow \infty} \frac{\sum_{d=1}^D w_d \delta_{t_d}(A_n) \hat{h}_j(t_d) + \int_{A_n} \hat{h}_j d\lambda}{\sum_{d=1}^D w_d \delta_{t_d}(A_n) + \lambda(A_n)}.$$

If there exists a $d_0 \in \{1, \dots, D\}$ with $s = t_{d_0}$, the term simplifies to the discrete case. Otherwise, the term simplifies to the continuous case. In both cases, the limit is $\hat{h}_j(s)$. \square

Proposition A.5. *If there exist subsets $I_t, I_s \subset I$ such that $\frac{\hat{h}_j(t)}{\hat{h}_j(s)} < \frac{\hat{h}_k(t)}{\hat{h}_k(s)}$ for all $t \in I_t, s \in I_s$, then,*

$$\frac{\mathbb{P}_j(I_t)}{\mathbb{P}_j(I_s)} < \frac{\mathbb{P}_k(I_t)}{\mathbb{P}_k(I_s)}. \quad (\text{A.10})$$

¹In practice, this is the case, when choosing continuous basis functions \mathbf{b}_Y like B-splines (for the continuous component).

Proof. Let $I_t, I_s \subset I$ such that $\frac{\hat{h}_j(t)}{\hat{h}_j(s)} < \frac{\hat{h}_k(t)}{\hat{h}_k(s)}$ for all $t \in I_t, s \in I_s$. Since \hat{h}_j, \hat{h}_k are μ -a.e. positive, this is equivalent to $\hat{h}_j(t)\hat{h}_k(s) < \hat{h}_j(s)\hat{h}_k(t)$. Integrating over $I_s \times I_t$ yields

$$\int_{I_s \times I_t} \hat{h}_j(t)\hat{h}_k(s) d(\mu \otimes \mu)(s, t) < \int_{I_s \times I_t} \hat{h}_j(s)\hat{h}_k(t) d(\mu \otimes \mu)(s, t).$$

By Tonelli's Theorem this factorizes and we get $\mathbb{P}_j(I_t)\mathbb{P}_k(I_s) < \mathbb{P}_j(I_s)\mathbb{P}_k(I_t)$, which gives us (A.10). \square

B Transforming a vector from $L^2(\mu)^{K_Y+1}$ to $L_0^2(\mu)^{K_Y}$

The approach described in this section is motivated by the inclusion of the sum-to-zero constraint in functional linear array models, compare (3.2), described in the online appendix A of Brockhaus et al. (2015). It is based on the implementation of linear constraints (Wood, 2017, Section 1.8.1). For a vector $\mathbf{b}_Y = (\bar{b}_{Y,1}, \dots, \bar{b}_{Y,K_Y+1}) \in L^2(\mu)^{K_Y+1}$, consider

$$\mathbf{C} := \left(\int_{\mathcal{T}} \bar{b}_{Y,1} d\mu, \dots, \int_{\mathcal{T}} \bar{b}_{Y,K_Y+1} d\mu \right) \in \mathbb{R}^{1 \times K_Y+1}.$$

Determining the QR decomposition of \mathbf{C}^\top yields

$$\mathbf{C}^\top = [\mathbf{Q} : \mathbf{Z}] \begin{bmatrix} R \\ \mathbf{0}_{K_Y} \end{bmatrix},$$

where $[\mathbf{Q} : \mathbf{Z}]$ is a $(K_Y + 1) \times (K_Y + 1)$ orthogonal matrix, R is a 1×1 (upper triangular) matrix and $\mathbf{0}_{K_Y}$ is the vector of length K_Y containing zeros in every component. The matrix $\mathbf{Z} = (z_{ij})_{i=1, \dots, K_Y+1, j=1, \dots, K_Y}$ is the desired transformation matrix. We obtain the transformed vector $\mathbf{b}_Y = (\tilde{b}_{Y,1}, \dots, \tilde{b}_{Y,K_Y})$ by the linear combinations of each column of \mathbf{Z} with the vector $\bar{\mathbf{b}}_Y$:

$$\tilde{b}_{Y,m} := \sum_{i=1}^{K_Y+1} \bar{b}_{Y,i} z_{im} \quad m = 1, \dots, K_Y$$

Then, we have

$$\begin{aligned} \left(\int_{\mathcal{T}} \tilde{b}_{Y,1} d\mu, \dots, \int_{\mathcal{T}} \tilde{b}_{Y,K_Y} d\mu \right) &= \left(\int_{\mathcal{T}} \sum_{i=1}^{K_Y+1} \bar{b}_{Y,i} z_{i1} d\mu, \dots, \int_{\mathcal{T}} \sum_{i=1}^{K_Y+1} \bar{b}_{Y,i} z_{iK_Y} d\mu \right) \\ &= \left(\sum_{i=1}^{K_Y+1} \int_{\mathcal{T}} \bar{b}_{Y,i} d\mu z_{i1}, \dots, \sum_{i=1}^{K_Y+1} \int_{\mathcal{T}} \bar{b}_{Y,i} d\mu z_{iK_Y} \right) \\ &= \mathbf{CZ} = [R : \mathbf{0}_{K_Y}^\top] \begin{bmatrix} \mathbf{Q}^\top \\ \mathbf{Z}^\top \end{bmatrix} \mathbf{Z} \\ &= [R : \mathbf{0}_{K_Y}^\top] \begin{bmatrix} \mathbf{0}_{K_Y}^\top \\ \mathbf{I}_{K_Y} \end{bmatrix} = \mathbf{0}_{K_Y}^\top, \end{aligned}$$

i.e., $\tilde{\mathbf{b}}_Y \in L_0^2(\mu)^{K_Y}$. Now let $\bar{\mathbf{b}}_Y \in L^2(\mu)^{K_Y+1}$ be a vector of basis functions with penalty matrix $\bar{\mathbf{P}}_Y \in \mathbb{R}^{(K_Y+1) \times (K_Y+1)}$. Then, the penalty matrix $\tilde{\mathbf{P}}_Y \in \mathbb{R}^{K_Y \times K_Y}$ for the transformed basis $\tilde{\mathbf{b}}_Y \in L_0^2(\mu)^{K_Y}$ is obtained by transforming the original penalty matrix: $\tilde{\mathbf{P}}_Y = \mathbf{Z}^\top \bar{\mathbf{P}}_Y \mathbf{Z}$.

C Equivalence of Boosting in $B^2(\mu)$ and $L_0^2(\mu)$

To explain the equivalence of boosting in $B^2(\mu)$ and boosting in $L_0^2(\mu)$, we briefly summarize how the gradient boosting algorithm in $B^2(\mu)$ as described in Section 3.2 is adapted for boosting in $L_0^2(\mu)$. Obviously, all functions that are elements of $B^2(\mu)$ in the original model and algorithm are considered elements of $L_0^2(\mu)$ for this purpose. In the following, we denote the latter functions with a tilde to distinguish them from the former ones. Furthermore, the Bayes Hilbert space operations \oplus, \odot and \otimes are replaced by their $L_0^2(\mu)$ -counterparts $+, \cdot$ and \otimes .

We take a closer look at the second and third steps of the algorithm, which are crucial for the equivalence of the two algorithms. In $L_0^2(\mu)$, they translate to:

2. Calculate the negative gradient (with respect to the Fréchet differential) of the empirical risk

$$\tilde{U}_i := -\nabla \rho_{\tilde{y}_i}(\tilde{f}) \Big|_{\tilde{f}=\widetilde{\hat{h}^{[m]}(\mathbf{x}_i)}} = 2 \left(\tilde{y}_i - \widetilde{\hat{h}^{[m]}(\mathbf{x}_i)} \right) \in L_0^2(\mu), \quad (\text{C.1})$$

where $\widetilde{\hat{h}^{[m]}(\mathbf{x}_i)} = \sum_{j=1}^J \left(\mathbf{b}_j(\mathbf{x}_i)^\top \otimes \tilde{\mathbf{b}}_Y^\top \right) \boldsymbol{\theta}_j^{[m]} \in L_0^2(\mu)$ and $\rho_{\tilde{y}_i} : L_0^2(\mu) \rightarrow \mathbb{R}, \tilde{f} \mapsto \|\tilde{y}_i - \tilde{f}\|_{L^2(\mu)}^2$ is the quadratic loss functional on $L_0^2(\mu)$. For $j = 1, \dots, J$, fit the base-learners

$$\hat{\boldsymbol{\zeta}}_j = \underset{\boldsymbol{\zeta} \in \mathbb{R}^{K_j K_Y}}{\operatorname{argmin}} \sum_{i=1}^N \left\| \tilde{U}_i - \left(\mathbf{b}_j(\mathbf{x}_i)^\top \otimes \tilde{\mathbf{b}}_Y^\top \right) \boldsymbol{\zeta} \right\|_{L^2(\mu)}^2 + \boldsymbol{\zeta}^\top \mathbf{P}_{jY} \boldsymbol{\zeta} \quad (\text{C.2})$$

and select the best base-learner

$$j^\star = \underset{j=1, \dots, J}{\operatorname{argmin}} \sum_{i=1}^N \left\| \tilde{U}_i - \left(\mathbf{b}_j(\mathbf{x}_i)^\top \otimes \tilde{\mathbf{b}}_Y^\top \right) \hat{\boldsymbol{\zeta}}_j \right\|_{L^2(\mu)}^2. \quad (\text{C.3})$$

3. The coefficient vector corresponding to the best base-learner is updated, the others stay the same: $\boldsymbol{\theta}_{j^\star}^{[m+1]} := \boldsymbol{\theta}_{j^\star}^{[m]} + \kappa \hat{\boldsymbol{\gamma}}_{j^\star}$, $\boldsymbol{\theta}_j^{[m+1]} := \boldsymbol{\theta}_j^{[m]}$ for $j \neq j^\star$.

The proof of the existence of the gradient and the equality in Equation (C.1) is analogous to the respective proof for the original algorithm, which is provided in appendix A.

Now we compare the estimation of the original model (3.1) applying the algorithm described in Section 3.2 with estimation of the clr transformed model

$$\operatorname{clr}[y_i] = \operatorname{clr}[h(\mathbf{x}_i)] + \operatorname{clr}[\varepsilon_i] = \sum_{j=1}^J \operatorname{clr}[h_j(\mathbf{x}_i)] + \operatorname{clr}[\varepsilon_i]. \quad (\text{C.4})$$

applying the adapted algorithm. Let $\mathbf{b}_Y = (b_{Y,1}, \dots, b_{Y,K_Y}) \in B^2(\mu)^{K_Y}$ be the vector of basis functions over \mathcal{T} in the original estimation problem. On clr transformed level, we choose $\tilde{\mathbf{b}}_Y = \text{clr}[\mathbf{b}_Y] = (\text{clr}[b_{Y,1}], \dots, \text{clr}[b_{Y,K_Y}]) \in L_0^2(\mu)^{K_Y}$ as the corresponding vector of basis functions over \mathcal{T} . Then, the negative gradient of the empirical risk in $L_0^2(\mu)$ equals the clr transformed negative gradient of the empirical risk in $B^2(\mu)$: Using the linearity of the clr transformation, we get

$$\begin{aligned} \text{clr}[\hat{h}^{[m]}(\mathbf{x}_i)] &= \text{clr} \left[\bigoplus_{j=1}^J \left(\mathbf{b}_j(\mathbf{x}_i)^\top \otimes \mathbf{b}_Y^\top \right) \boldsymbol{\theta}_j^{[m]} \right] \\ &= \sum_{j=1}^J \left(\mathbf{b}_j(\mathbf{x}_i)^\top \otimes \text{clr}[\mathbf{b}_Y]^\top \right) \boldsymbol{\theta}_j^{[m]} = \widetilde{\hat{h}^{[m]}(\mathbf{x}_i)}, \end{aligned}$$

and thus $\text{clr}[U_i] = \text{clr} \left[2 \odot (y_i \ominus \hat{h}^{[m]}(\mathbf{x}_i)) \right] = 2 \left(\text{clr}[y_i] - \text{clr}[\hat{h}^{[m]}(\mathbf{x}_i)] \right) = \tilde{U}_i$. Furthermore, for all $i = 1, \dots, N$, $j = 1, \dots, J$ and $\boldsymbol{\gamma} \in \mathbb{R}^{K_j K_Y}$, we have

$$\begin{aligned} \left\| U_i \ominus \left(\mathbf{b}_j(\mathbf{x}_i)^\top \otimes \mathbf{b}_Y^\top \right) \boldsymbol{\gamma} \right\|_{B^2(\mu)}^2 &= \left\| \text{clr} \left[U_i \ominus \left(\mathbf{b}_j(\mathbf{x}_i)^\top \otimes \mathbf{b}_Y^\top \right) \boldsymbol{\gamma} \right] \right\|_{L^2(\mu)}^2 \\ &= \left\| \tilde{U}_i - \left(\mathbf{b}_j(\mathbf{x}_i)^\top \otimes \tilde{\mathbf{b}}_Y^\top \right) \boldsymbol{\gamma} \right\|_{L^2(\mu)}^2. \end{aligned}$$

Here, we used the isometry of the clr transformation in the first equation and its linearity in the second one. This implies that the pairs of equations (3.6) and (C.2) and (3.7) and (C.3) yield the same result, i.e., $\hat{\boldsymbol{\gamma}}_j = \hat{\boldsymbol{\zeta}}_j$ for all $j = 1, \dots, J$ and $j^* = j^\star$, in each iteration of the two algorithms. This means that the update in the third step of both algorithms is identical as well. Thus, the resulting estimator of model (C.4) is the clr transformed estimator of (3.1):

$$\widehat{\text{clr}[y_i]} = \sum_{j=1}^J \widetilde{\hat{h}_j^{[m_{\text{stop}}]}(\mathbf{x}_i)} = \sum_{j=1}^J \text{clr} \left[\hat{h}_j^{[m_{\text{stop}}]}(\mathbf{x}_i) \right] = \text{clr} \left[\bigoplus_{j=1}^J \hat{h}_j^{[m_{\text{stop}}]}(\mathbf{x}_i) \right] = \text{clr}[\hat{y}_i].$$

This proves that the algorithms provide equivalent results: We obtain the same estimates by applying the adapted algorithm to the clr transformed model (C.4) in $L_0^2(\mu)$ and retransforming the estimates with clr^{-1} as by estimating model (3.1) directly in $B^2(\mu)$. An advantage of transforming the model is that we can then use and extend implementations for function-on-scalar regression in practice, in particular the R add-on package `FDboost` (Brockhaus and Rügamer, 2018), which is based on the package `mboost` (Hothorn et al., 2018). Our enhanced version of the package can be found in the github repository *FDboost*. The vignette “density-on-scalar_birth” illustrates how to use it for the density-on-scalar case.

D Further ideas for interpreting estimated effects

In addition to the approach of interpreting estimated effects via (log) odds ratios as presented in Section 3.4 and used in the application in Section 4, we developed the

following ideas for interpretation. Sections D.1 and D.2 extend the ideas of odds (ratios). Section D.3 presents a completely different approach, decomposing the domain \mathcal{T} into two areas where the probability mass of another density increases/decreases under perturbation with this effect.

D.1 Odds compared to geometric mean

While the odds of an effect $\hat{h}_j = \hat{h}_j^{[m_{\text{stop}}]}(\mathbf{x}_i) \in B^2(\mu)$, $j = 1, \dots, J$ for t compared to s , with $t, s \in \mathcal{T}$, are given by the exponential of the difference of the clr transformed effect evaluated at t and s , see (3.9), the exponential of the clr transformed effect at t can also be interpreted directly via the relation

$$\exp(\text{clr}[\hat{h}_j](t)) = \frac{\hat{h}_j(t)}{\exp \mathcal{S}(\hat{h}_j)},$$

where $\exp \mathcal{S}(\hat{h}_j)$ is the geometric mean of \hat{h}_j , see Section 3.3. Thus, the ratio on the right is called *odds of \hat{h}_j for t compared to the geometric mean*. The log odds ratio of two effects \hat{h}_j and \hat{h}_k , $j \neq k \in \{1, \dots, J\}$, for t compared to the geometric mean corresponds to the difference of the clr transformed effects at t . Again, it is not changed when adding effects $\hat{h}_{\mathcal{J}} = \bigoplus_{l \in \mathcal{J}} \hat{h}_l$ with $\mathcal{J} \subset \{1, \dots, J\} \setminus \{j, k\}$ to both, \hat{h}_j and \hat{h}_k (ceteris paribus).

D.2 Odds for mixed case

In the mixed case, i.e., $B^2(\mu) = B^2(I, \mathfrak{B}, \mu)$ with $\mu = \delta + \lambda$, where $\delta = \sum_{d=1}^D w_d \delta_{t_d}$ for $\{t_1, \dots, t_D\} = \mathcal{D} \subset I$ and $w_d > 0$, we get a special interpretation for the odds (as defined in (3.9)) of the discrete component of an effect: Let $\hat{h}_{j,d} \in B^2(\delta^\bullet)$ denote the function obtained from (3.8) given the effect $\hat{h}_j \in B^2(\mu)$. Then, for the odds of a discrete value $t \in \mathcal{D}$ compared to the value t_{D+1} representing the continuous component, we get

$$\frac{\hat{h}_{j,d}(t)}{\hat{h}_{j,d}(t_{D+1})} \stackrel{(3.8)}{=} \frac{\hat{h}_j(t)}{\mathcal{S}_\lambda(\hat{h}_j)}.$$

Thus, for the discrete component $\hat{h}_{j,d}$ the odds of $t \in \mathcal{D}$ compared to t_{D+1} correspond to the odds of the relative frequency of $t \in \mathcal{D}$ compared to the geometric mean of the continuous component. It is given by the exponential of the differences of the $\text{clr}_{\delta^\bullet}$ transformed effect $\hat{h}_{j,d}$ evaluated at t and t_{D+1} .

D.3 Decomposition of \mathcal{T} depending on constant

The following statement applies to all Bayes Hilbert spaces $B^2(\mathcal{T}, \mathcal{A}, \mu) = B^2(\mu)$, in particular to the discrete, continuous and mixed cases. It implies that any positive constant α decomposes an effect $g \in B^2(\mu)$ into an area $I = \{g \geq \alpha\}$, where the probability mass of an arbitrary density $f \in B^2(\mu)$ increases under perturbation with g and an area $I^c = \{g < \alpha\}$ where the probability mass decreases. Note that

this statement requires I to be the maximal subset with $g \geq \alpha$. If we don't presume $g < \alpha$ on I^c , this is not true in general.

Since we are interested in probability masses, we consider probability density functions in the following.

Theorem D.1. *Let $f, g \in B^2(\mu)$ with $\int_{\mathcal{T}} f \, d\mu = 1 = \int_{\mathcal{T}} g \, d\mu$ and $g \geq \alpha$ on $I \subseteq \mathcal{T}$ and $g < \alpha$ on $I^c = \mathcal{T} \setminus I$ for $\alpha \in \mathbb{R}^+$. Then,*

$$\int_I f \oplus g \, d\mu \geq \int_I f \, d\mu \quad (\text{D.1})$$

and

$$\int_{I^c} f \oplus g \, d\mu \leq \int_{I^c} f \, d\mu. \quad (\text{D.2})$$

Proof. We have

$$\int_I f \oplus g \, d\mu = \frac{\int_I f \cdot g \, d\mu}{\int_{\mathcal{T}} f \cdot g \, d\mu} = \frac{\int_I f \cdot g \, d\mu}{\int_I f \cdot g \, d\mu + \int_{I^c} f \cdot g \, d\mu}$$

and analogously

$$\int_{I^c} f \oplus g \, d\mu = \frac{\int_{I^c} f \cdot g \, d\mu}{\int_I f \cdot g \, d\mu + \int_{I^c} f \cdot g \, d\mu}.$$

Consider

$$a := \int_I f \, d\mu, \quad b := \int_I f \cdot g \, d\mu, \quad c := \int_{I^c} f \cdot g \, d\mu.$$

Since $g \geq \alpha$ on I and $g < \alpha$ on I^c , we have

$$(I) \quad b \geq \alpha \cdot a$$

$$(II) \quad c < \alpha \cdot (1 - a) = \alpha - \alpha \cdot a$$

Note that $a \in [0, 1]$ and $b, c \geq 0$ with $b + c > 0$. If $a = 1$, we have $I = \mathcal{T}$ and $I^c = \emptyset$. Then, equality is reached in both (D.1) and (D.2), since both sides are 1 and 0, respectively. If $a = 0$, we have $I = \emptyset$ and $I^c = \mathcal{T}$ and again (D.1) and (D.2) hold with equality reached. Now, consider $a \in (0, 1)$. Assume (D.1) is not true, i.e., $\frac{b}{b+c} < a$. Then, we have

$$\begin{aligned} \frac{b}{b+c} < a &\Leftrightarrow b < a \cdot (b+c) \stackrel{(II)}{\implies} b < a \cdot (b + \alpha - \alpha \cdot a) \\ &\Leftrightarrow b \cdot (1-a) < \alpha \cdot a \cdot (1-a) \stackrel{a < 1}{\iff} b < \alpha \cdot a, \end{aligned}$$

which is a contradiction to (I). Thus, $\frac{b}{b+c} \geq a$, which shows (D.1). This also implies $\frac{c}{b+c} = 1 - \frac{b}{b+c} \leq 1 - a$, which shows (D.2). \square

²Note that using a similar approach as above, starting with the assumption $\frac{c}{b+c} \geq 1 - a$ and using (I) to obtain a contradiction to (II), one can even show the strict inequality $\frac{c}{b+c} < 1 - a$ for $a \in (0, 1)$.

E Application: Women's income share

We use data from the German Socio-Economic Panel (SOEP) from 1984 to 2016 (version 33, doi:10.5684/soep.v33, see Goebel et al. (2019)), with data for *East* Germany being available only from 1991 onward.

E.1 Overview of regions

Federal state	ISO 3166-2 code	region	West_East
Schleswig-Holstein	SH	northwest	West (Germany)
Bremen	HB		
Hamburg	HH		
Lower Saxony	NI		
North Rhine-Westphalia	NW	west	
Hesse	HE	southwest	
Rhineland-Palatinate	RP		
Saarland	SL		
Bavaria	BY	south	
Baden-Württemberg	BW		
Saxony-Anhalt	ST	east	East (Germany)
Thuringia	TH		
Saxony	SN		
Berlin	BE	northeast	
Brandenburg	BB		
Mecklenburg-West Pomerania	MV		

Table E.1: German federal states with their ISO 3166-2 codes and the variables *region* and *West_East* assigned in our application.

E.2 Barplots of share frequencies

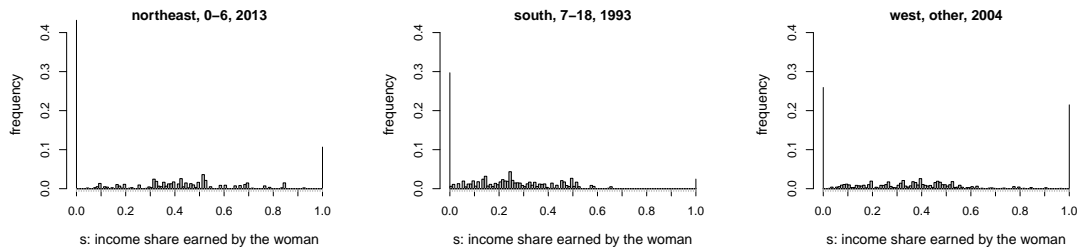


Figure E.1: Three barplots of share frequencies for different combinations of *region*, *c_age*, and *year*. The outmost bars have width zero, the ones in between width 0.01.

E.3 Estimation of the response densities

In practice, density functions often have to be estimated from individual observations. We focus on densities with bounded support \mathcal{T} , which is predetermined by the

application framework. Without loss of generality, we assume $\mathcal{T} = [0, 1]$ as support of the unknown density f , which has to be estimated.

A common approach to estimate densities is kernel density estimation. The usual kernel density estimator for weighted observations is

$$\hat{f}_b(t) := \sum_{l=1}^N w_l K_b(t - t_l), \quad (\text{E.1})$$

where $t_1 \leq \dots \leq t_N$ is a random sample of a random variable T with (unknown) density f , w_1, \dots, w_N with $\sum_{l=1}^N w_l = 1$ are corresponding nonnegative weighting coefficients (sampling weights in our application to ensure representativeness of the survey) and K_b is a kernel function depending on a bandwidth $b \in \mathbb{R}$. Usually, kernel functions fulfill $K_b(t) = K\left(\frac{t}{b}\right)$, where K is chosen as a density function that is symmetric around zero. However, this is not suitable, when the bounded support \mathcal{T} of the estimator is predetermined: If the support of K is unbounded, which is the case for, e.g., the Gaussian kernel, the support of the estimator is unbounded as well. If the support of K is bounded, i.e., $[-a, a]$ for an $a > 0$, the support of the estimator is $\left[\frac{t_1 - a}{b}, \frac{t_N + a}{b}\right]$ (assuming $t_l - t_{l-1} < 2a$ for all $l = 1, \dots, N$). Thus, it is not fixed, but depends on the sample t_1, \dots, t_N and doesn't necessarily yield the predefined $\mathcal{T} = [0, 1]$.

To accommodate this, there are several possibilities. Petersen and Müller (2016) propose a new kernel density estimator based on symmetric kernels. Outside of the predetermined interval, the value is set to 0. Normalization ensures that the estimator integrates to 1 and a so-called weight function, which depends on t , the bandwidth, and the kernel and is unequal to 1 only in $[0, b)$ and $(1 - b, 1]$, is multiplied with the kernel to remove boundary bias. Another possibility is to use the usual kernel density estimator, but with asymmetric kernels, which are defined on the predetermined interval. Two appropriate choices are beta-kernels introduced by Chen (1999) and Gaussian copula kernels presented by Jones and Henderson (2007). The former are also recommended by Petersen and Müller (2016) as alternative to their own estimation approach. Both kernels are illustrated in Figure E.2 for bandwidths 0.02 and 0.1. Besides obviously different scaling of the bandwidth parameter, the two kernels show very different behavior near the boundaries of the interval $[0, 1]$.

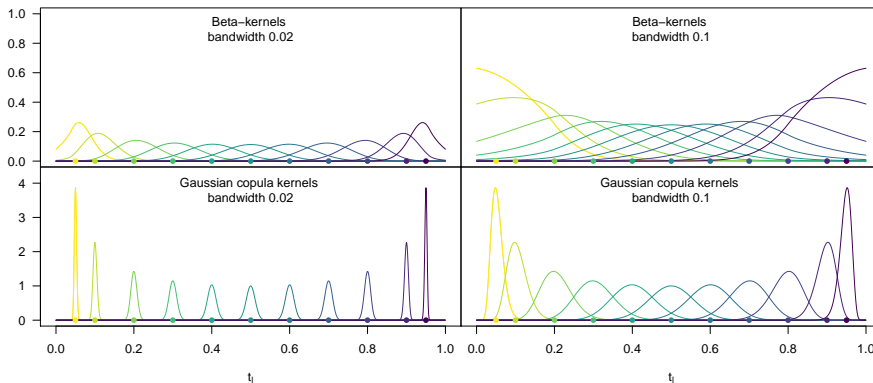


Figure E.2: Beta-kernels [top] and Gaussian copula kernels [bottom] for the bandwidths 0.02 [left] and 0.1 [right] for different values of t_l .

In our application we use beta-kernels due to better results. Chen (1999) actually presents two versions of beta-kernels, of whom we use the second one, which is also the one depicted in Figure E.2. It has reduced bias compared to the first and is defined as

$$\hat{f}_b^*(t) := \sum_{l=1}^N w_l K_{t,b}^*(t_l) \quad (\text{E.2})$$

for $t \in [0, 1]$ with kernel functions

$$K_{t,b}^*(x) := \begin{cases} K_{\rho(t,b), (1-t)/b}(x), & t \in [0, 2b) \\ K_{t/b, (1-t)/b}(x), & t \in [2b, 1-2b] \\ K_{t/b, \rho(1-t,b)}(x), & t \in (1-2b, 1], \end{cases}$$

where $\rho(t, b) := 2b^2 + 2.5 - \sqrt{4b^4 + 6b^2 + 2.25 - t^2 - t/b}$ and $K_{p,q}$ denotes the density function of a Beta(p, q)-distribution. We slightly modified the original definition of the estimator \hat{f}_b^* by including weighting coefficients w_l to match the setting in our application. Chen (1999) uses equal weights, i.e., $w_l = \frac{1}{N}$ for all $l = 1, \dots, N$. Note that the resulting estimator usually does not integrate to one as the functions $K_{t,b}^*(x)$ are only probability density functions in x but not in t . Therefore, a normalization is necessary to get the estimated density³:

$$\hat{f}_b(t) := \frac{\hat{f}_b^*(t)}{\int_0^1 \hat{f}_b^*(t) dt}. \quad (\text{E.3})$$

The optimal bandwidth b can be chosen with unbiased cross-validation (e.g., Scott, 2015). This is also the default to choose the bandwidth for asymmetric kernels in the R package `kdensity` (Moss and Tveten, 2018), where both beta-kernels and Gaussian copula kernels are implemented, amongst others.

In our application, for each unique combination of covariate values we compute a density $f_{(0,1)} : (0, 1) \rightarrow \mathbb{R}^+$ using beta-kernels based on dual-earner households. To determine the bandwidth, we calculate the optimal bandwidth for each of the 552 densities with unbiased cross-validation and choose the minimal resulting bandwidth as final bandwidth for all densities, yielding a value of 0.02. Selecting a smaller bandwidth prevents us from over-smoothing, which may disguise possible effects. Furthermore, a small bandwidth allows for steep gradients, which indicate a possible discontinuity⁴. Using the estimated densities $f_{(0,1)}$ on $(0, 1)$, we obtain the response

³As \hat{f}_b^* and \hat{f}_b are proportional, they are ($=_{\mathcal{B}}$)-equivalent λ -densities with λ denoting the Lebesgue measure. But in accordance to usual probability density functions, we use the density as representative that integrates to one.

⁴Bertrand et al. (2015) consider the share of the wife's income in a couple's total income for married couples in the U.S. and infer that there is a sharp discontinuous drop to the right of 0.5. This is in general not confirmed by our data, but we chose a small bandwidth to ensure flexibility of density estimation to capture such a decline.

densities on $[0, 1]$ as

$$f : [0, 1] \rightarrow \mathbb{R}^+ \quad s \mapsto \begin{cases} p_0, & s = 0 \\ p_{(0,1)} f_{(0,1)}(s), & s \in (0, 1) \\ p_1, & s = 1, \end{cases} \quad (\text{E.4})$$

where p_0 and p_1 are the relative frequencies for a share of 0 and 1, respectively, and $p_{(0,1)} = 1 - p_0 - p_1$ is the relative frequency for a share in $(0, 1)$.

E.4 Sensitivity Check for varying base-learner degrees of freedom

In this section, we give some insights leading to the decision to use a model which is theoretically unfair regarding base-learner selection. First, we perform a sensitivity check comparing it with a model that is fair in the sense that the *West_East* effect base-learner does have the same number of degrees of freedom as other base-learners in the model. Afterwards, we compare the resulting predictions with the response densities, revealing that the unfair model shows a better fit to the data than the fair one. Note that both models are estimated with the R package *FDboost*, which uses effect coding. To improve interpretability, we converted those to reference coding for the application. However, base-learner selection is performed by *FDboost* on effect coded level, thus we consider effect coding in the following. For simplicity, we still use the denotation $\hat{\beta}_{...}, \hat{g}_{...}(year)$ even though these effects are not identical to the reference coded effects denoted like this in the remaining paper.

To ensure a fair selection process within the gradient boosting algorithm, each base-learner should ideally have the same number of degrees of freedom. In our model (4.1), this is not possible for the covariate effects, as the flexible nonlinear effects need a minimum of 2 degrees of freedom, while the intercept β_0 and β_{West_East} only allow for a maximal value of 1. Regarding base-learner selection, β_{West_East} thus is theoretically at a disadvantage compared to the other main effects. To study the severity of this disadvantage, we compare our model with another model, which is fair regarding base-learner selection. This is reached by dividing the degrees of freedom in direction of the share in half for all effects but β_0 and β_{West_East} , in both, the continuous and discrete model. Apart from that, the models are specified identically to the ones presented in the main manuscript. Again, we determine the stopping iterations based on 25 bootstrap samples, respectively, resulting in 490 for the continuous and 735 for the discrete model. For simplicity, we refer to the resulting models as *fair* models in contrast to the *unfair* models of choice in the following. In our sensitivity check, we first compare the selection frequencies, the crucial parameter for the fairness of a model. For further insights, we also consider the in-bag risk reduction and the estimated effects for β_{West_East} in the fair vs. the unfair models.

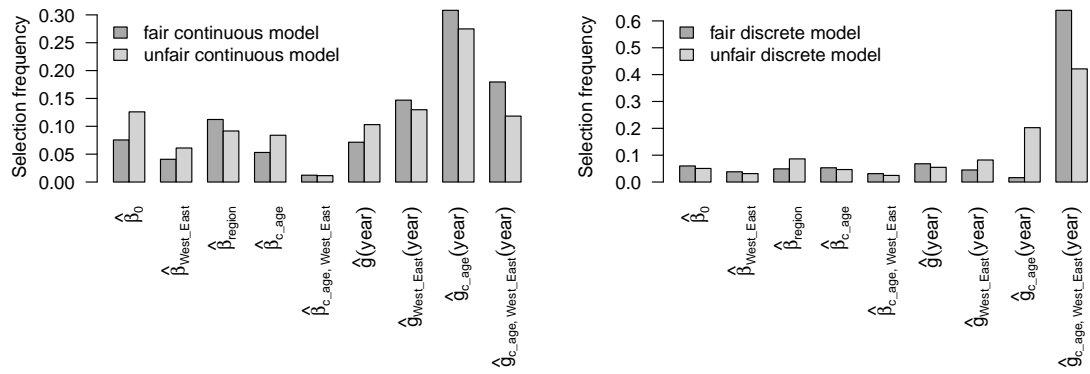


Figure E.3: Selection frequencies of the different (effect coded) effects for fair vs. unfair models for continuous [left] and discrete [right].

Figure E.3 shows the selection frequencies of each effect in the continuous and discrete models comparing the fair with the unfair models, respectively. The left side shows the continuous models. Here, β_{West_East} gets selected even more often in the unfair model – where it is theoretically disadvantaged – than in the fair model. Considering the discrete models (right), β_{West_East} is selected slightly less often than in the fair model, but the difference does not seem severe.

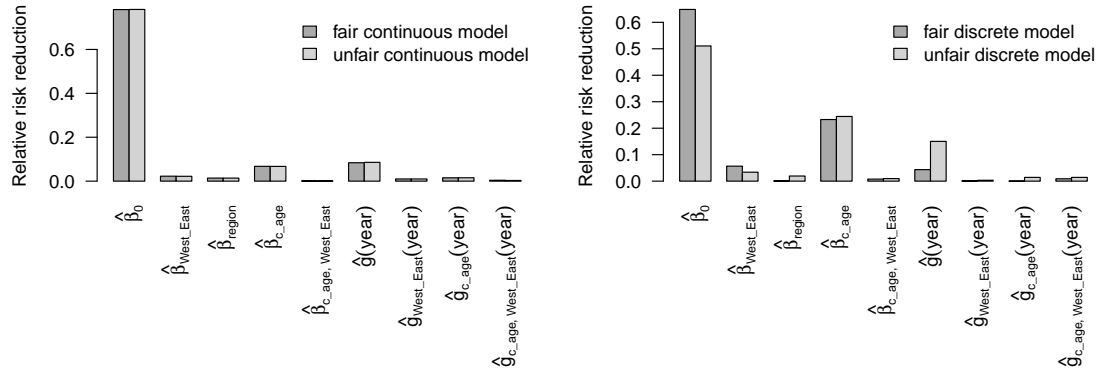


Figure E.4: Relative in-bag risk reduction of the different (effect coded) effects for fair vs. unfair models for continuous [left] and discrete [right].

The relative in-bag risk reduction of the effects in the different models is illustrated in Figure E.4. For the continuous models (left), the risk reductions per effect are almost identical in both models, which indicates that there is no disadvantage for β_{West_East} in the unfair model. For the discrete models (right), β_{West_East} again deems more important in the fair model than in the unfair one.

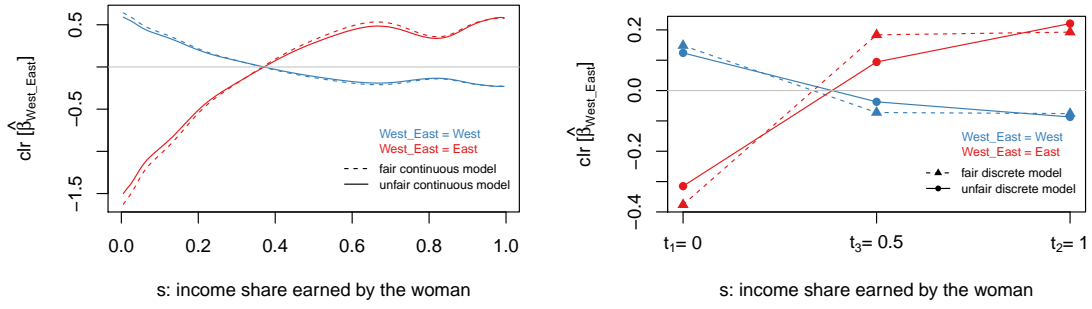


Figure E.5: Clr transformed estimated (effect coded) effects of $West_East$ for fair vs. unfair models for continuous [left] and discrete [right].

Finally, we compare the clr transformed estimated effects of β_{West_East} in the different models in Figure E.5. While this does not allow conclusions about the fairness of the models, it might be disconcerting, if the estimated effects were completely different. However, this is not the case. We obtain very similar effects in the continuous models (left). Regarding the discrete models (right), the values differ more (relatively), but the trend is the same.

In summary, we observe almost no differences in the continuous models between a fair and unfair model specification. In contrast, there are slight differences in the discrete models. However, they are not too severe, so that β_{West_East} does not seem to be at a large disadvantage.

We decided to prefer the unfair model to the fair one because of the fit to the data. Figure E.6 shows the predicted densities resulting from the fair model, Figure E.7 the response densities, and Figure E.8 the predicted densities resulting from the unfair model. All three figures are structured as follows. In the upper part, they illustrate the respective densities for all six *regions* and all three *c_age* groups. The densities are shown in one panel for all *years*, respectively, with a color gradient and different line types indicating the *year*. The density values at the boundaries 0 and 1 are represented as dashes, shifted slightly outwards for better visibility. The lower part of the figures show their development over time more clearly. For the response densities (Figure E.7), they are represented as dashes again (green and red, respectively), while the relative frequency of dual-earner households is illustrated via blue circles. For the predicted densities (Figures E.6 and E.8), the smooth trend over time is shown by different types of lines, but using the same colors as for the response densities.

First, we compare the predictions from the fair model, i.e., Figure E.6, with the response densities, i.e., Figure E.7. In general, the shapes of the predicted densities for $s \in (0, 1)$ match the ones of the response densities for the different *regions* and values of *c_age* (upper parts of the figures): The densities corresponding to *regions* in West Germany (*northeast*, *west*, *southwest*, *south*) show more probability mass at smaller income shares for couples with minor children (*0-6* and *7-18*) compared to couples without minor children (*other*), while the densities for East Germany (*east*, *northeast*) show more symmetric distributions regardless of the age of the youngest child. However, the absolute values of the predicted densities resulting from the fair model are at the same level for couples with children aged 0-6 years as for couples with children aged 7-18 years. Regarding the response densities, this is not the case.

Here, the absolute values of the densities corresponding to $0-6$ are lower than the ones for $7-18$. Furthermore, the trend over the years is not covered well, especially in the discrete model, which shows in the relative frequencies (lower part of the figures): For the predicted densities resulting from the fair models, we expect an increase of non-working women (p_0) and a decrease of dual-earner households ($p_{(0,1)}$) with time in all regions and for all values of c_age . For the response densities, these developments are the other way around: p_0 tends to decrease, while $p_{(0,1)}$ tends to increase! In contrast, comparing the predicted densities resulting from the unfair model (Figure E.8) with the response densities (Figure E.7), these issues do not appear, while the shapes of the predicted densities in $s \in (0, 1)$ are still matched nicely. Finally, we consider the sum of squared errors (SSE) as defined in (3.3) for both models. It also leads to the decision to prefer the unfair model as its SSE is only 1436 and thus smaller than the SSE of the fair model, which is 1704.

Apparently, the fair model is not flexible enough to fit the data well due to the reduced degrees of freedom for the basis over $(0, 1)$ for the continuous model and over $\{0, 1, 0.5\}$ for the discrete one. Thus, we decided to discard the fair model and keep the unfair one instead.

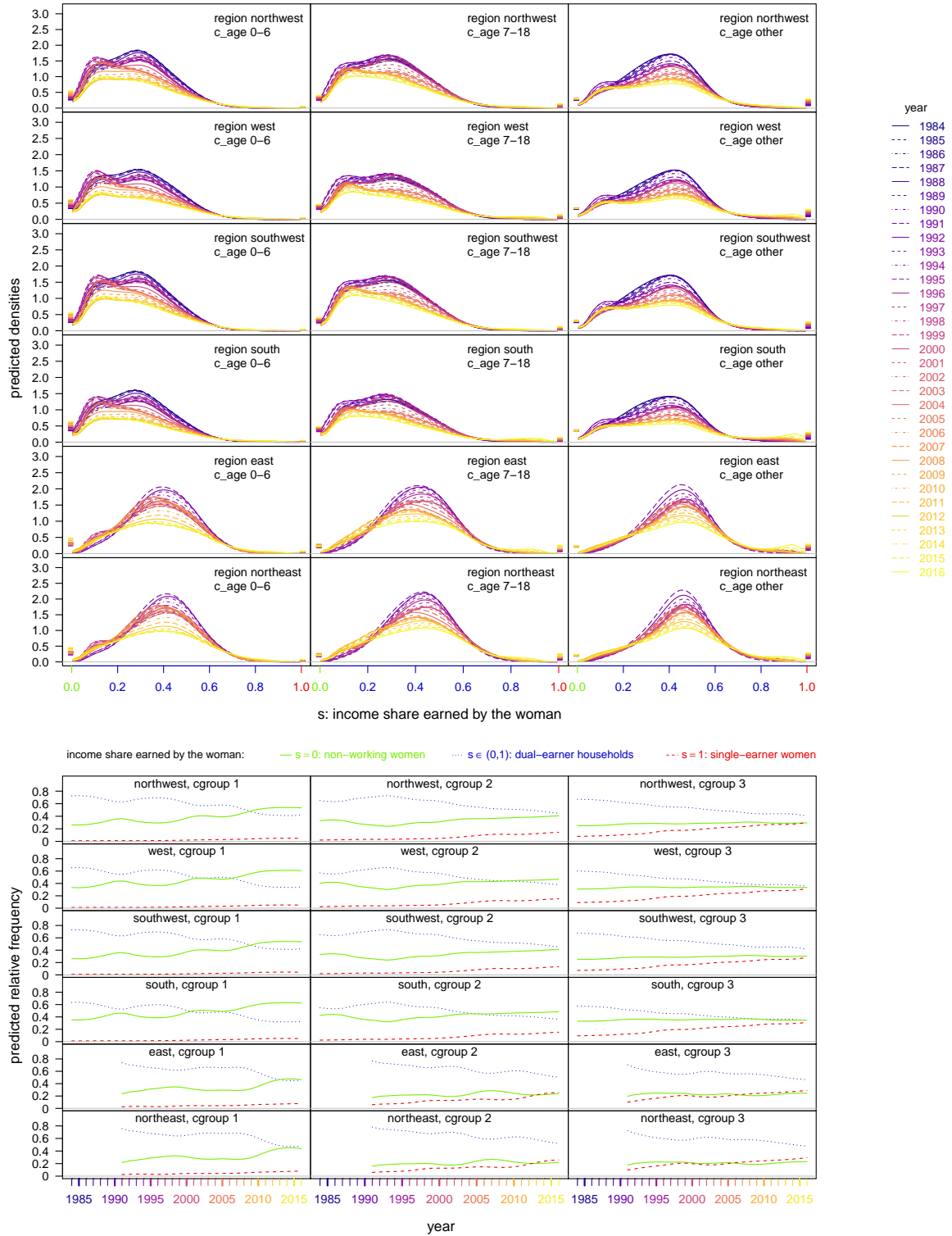


Figure E.6: Predicted densities [upper 6×3 panels] and corresponding relative frequencies [lower 6×3 panels] resulting from finally discarded fair models for all *regions* [rows] for all three values of *c_age* [columns].

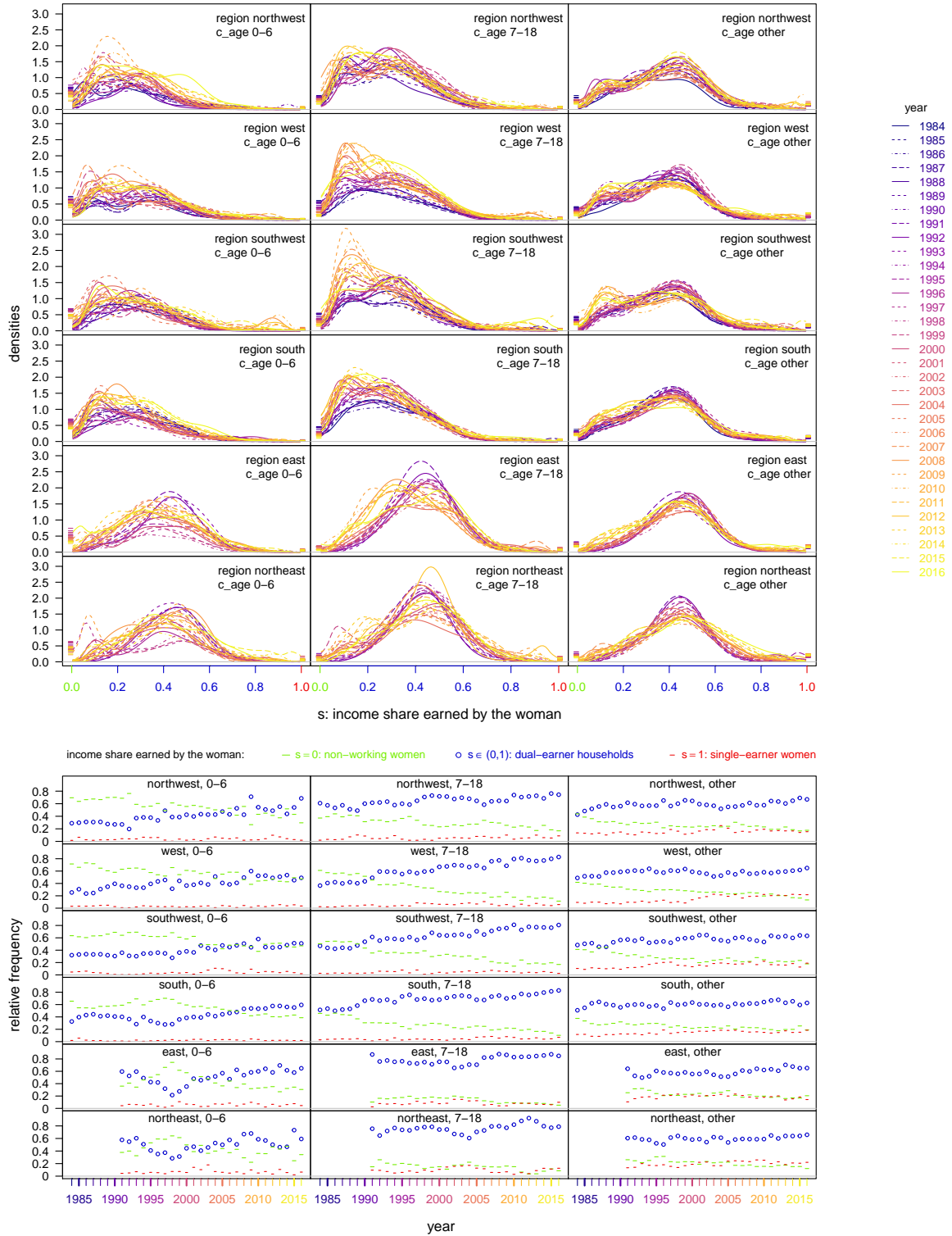


Figure E.7: Response densities [upper 6×3 panels] and corresponding relative frequencies [lower 6×3 panels] for all *regions* [rows] for all three values of *c_age* [columns].

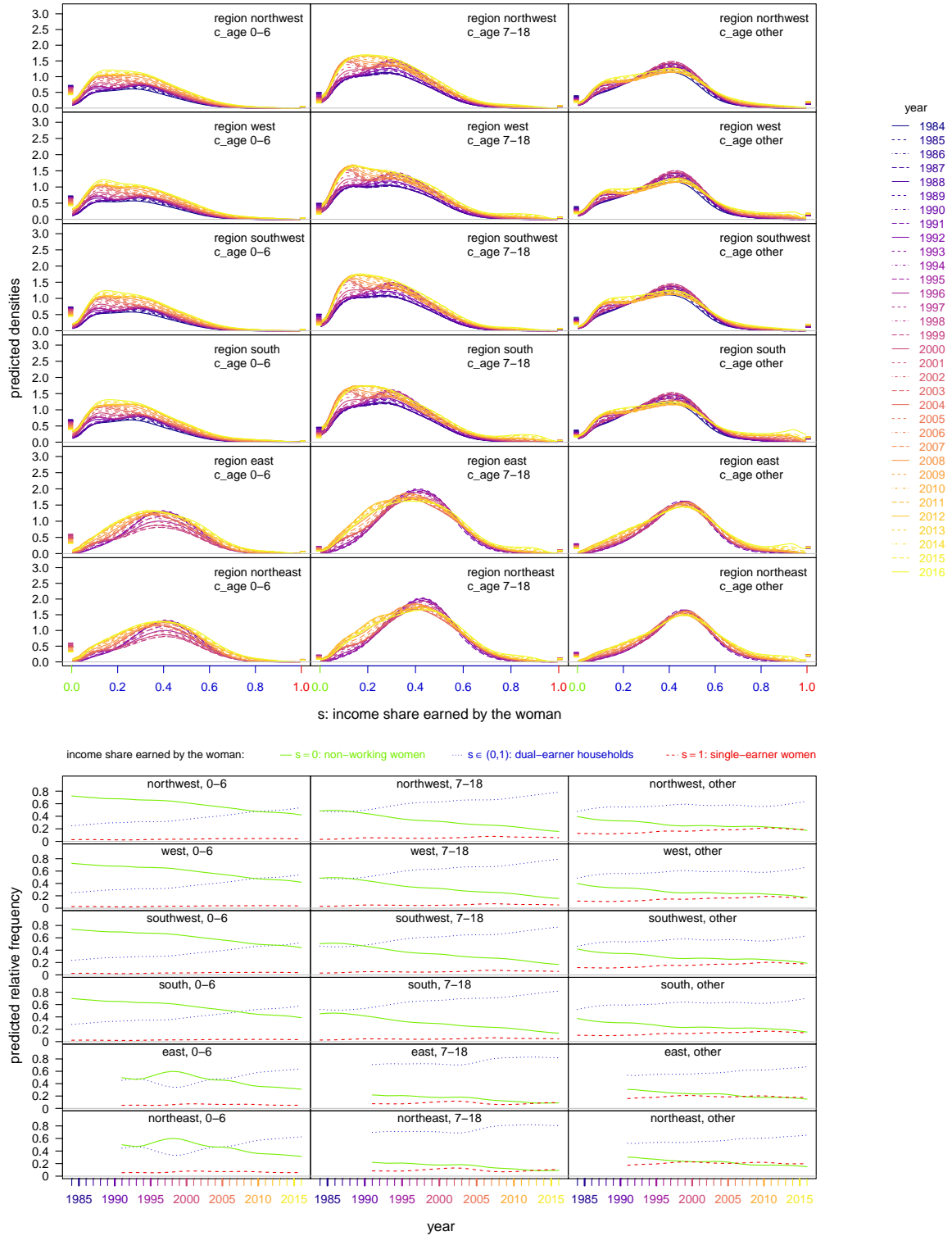


Figure E.8: Predicted densities [upper 6×3 panels] and corresponding relative frequencies [lower 6×3 panels] resulting from finally used unfair models for all *regions* [rows] for all three values of *c_age* [columns].

E.5 Estimated Effects

This section shows all estimated effects of model (4.1) with Figures E.9-E.16 structured similar to Figure 4.2. The left side shows the perturbation of the intercept with the respective effect and other reasonable effects (e.g., the main effects for interaction effects). The circles at 0.5 correspond to the Lebesgue integral of the respective function, i.e., the expected relative frequency of dual-earner households. On the right side, we illustrate the clr transformed effects to easily allow their interpretation via (log) odds ratios as described in Section 3.4. Example interpretations are given for Figures E.9 and E.13.

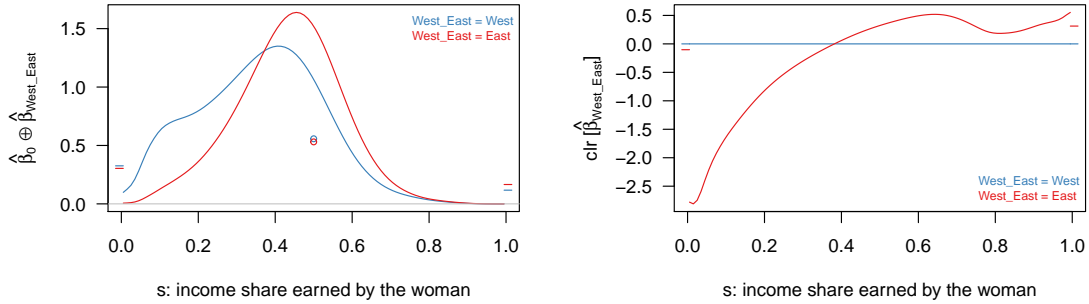


Figure E.9: Expected densities for couples without minor children in 1991 for *West* vs. *East* Germany [left] and clr transformed estimated effects of *West_East* [right].

Figure E.9 illustrates the estimated effect of *West_East*. As *West* is the reference category, we have $\hat{\beta}_0 \oplus \hat{\beta}_{West} = \hat{\beta}_0$ and $\text{clr}[\hat{\beta}_{West}] = 0$. The left part of the figure shows the expected densities for couples living in *West* versus *East* Germany for the reference, i.e., couples without minor children in 1991. For *West* Germany, the expected density over $(0, 1)$ has a smaller mode and probability mass shifted to the left compared to *East* Germany. Non-working women ($s = 0$) are more frequent in *West* than in *East* Germany, while dual-earner households (circles at $s = 0.5$) and single-earner women ($s = 1$) are more frequent in *East* Germany. Alternatively, we can interpret the log odds ratio of $\hat{\beta}_{East}$ and $\hat{\beta}_{West}$ for t compared to s for any $s, t \in [0, 1]$ of interest (right). It equals the log odds of $\hat{\beta}_{East}$, i.e., $\text{clr}[\hat{\beta}_{East}](t) - \text{clr}[\hat{\beta}_{East}](s)$, corresponding to vertical differences in the red curve. First, we compare the boundary values, i.e., single-earner households. The log odds ratio for $t = 1$ compared to $s = 0$ is $0.31 - (-0.44) = 0.75$, which means that the odds for single-earner versus non-working women in *East* Germany are $\exp(0.75) \approx 2.12$ times the odds in *West* Germany. To compare dual-earner households with non-working women, consider the log odds ratio for $t \in (0, 1)$ and $s = 0$, which is negative for $t < 0.23$ and positive otherwise. E.g., the log odds ratio for $t = 0.5$ compared to $s = 0$ is $0.53 - (-0.44) = 0.97$, i.e., the odds for equal earning couples versus non-working women in *East* Germany are $\exp(0.97) \approx 2.64$ times the odds in *West* Germany. The log odds ratio for $t = 1$ (single-earner women) compared to $s \in (0, 1)$ (dual-earner households) is positive for $s < 0.42$ and negative for larger s . E.g., for $s = 0.5$, the log odds ratio is $0.31 - 0.53 = -0.22$, i.e., the odds for single-earner women versus equal earning couples in *East* Germany are $\exp(-0.22) \approx 0.8$ times the odds in *West* Germany. Within dual-earner households, i.e., for $s, t \in (0, 1)$, the

log odds ratio of $\hat{\beta}_{East}$ and $\hat{\beta}_{West}$ for t compared to s is mostly positive for $s < t$ as $\text{clr}[\hat{\beta}_{East}]$ increases monotonically (except between 0.7 and 0.8). Thus, the odds for a larger versus a smaller income share are larger in *East* than in *West* Germany.

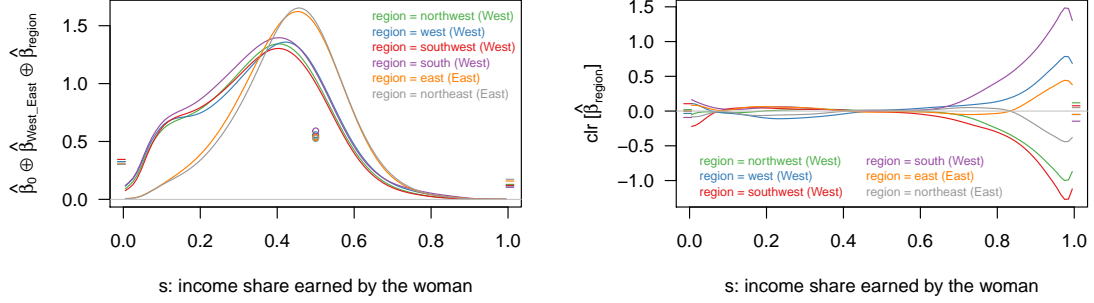


Figure E.10: Expected densities for couples without minor children in 1991 living in the different *regions* [left] and clr transformed estimated effects of *region* [right].

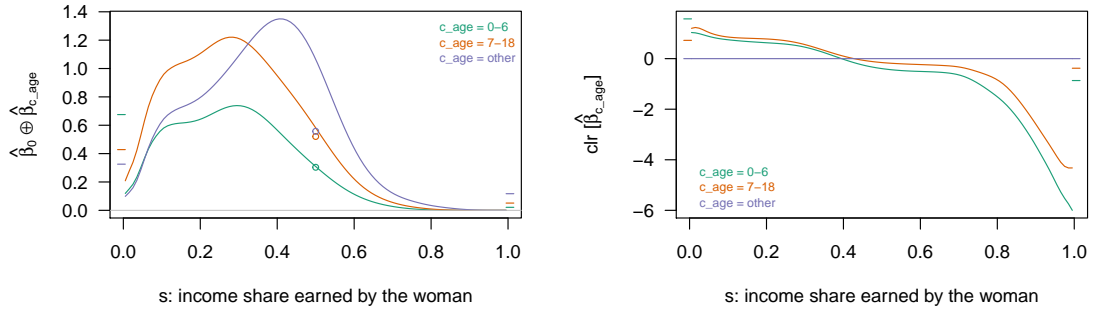


Figure E.11: Expected densities for couples living in *West* Germany in 1991 for all three values of c_age [left] and clr transformed estimated effects of c_age [right].

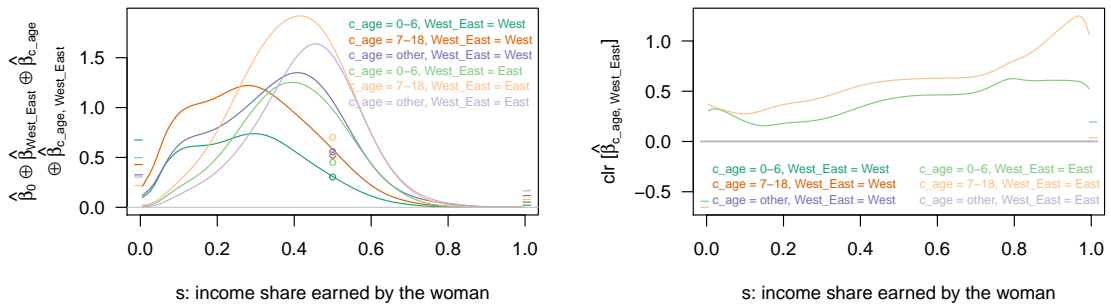


Figure E.12: Expected densities for couples in 1991 for all three values of c_age living in *West* vs. *East* Germany [left] and clr transformed estimated interaction effects of c_age and $West_East$ [right].

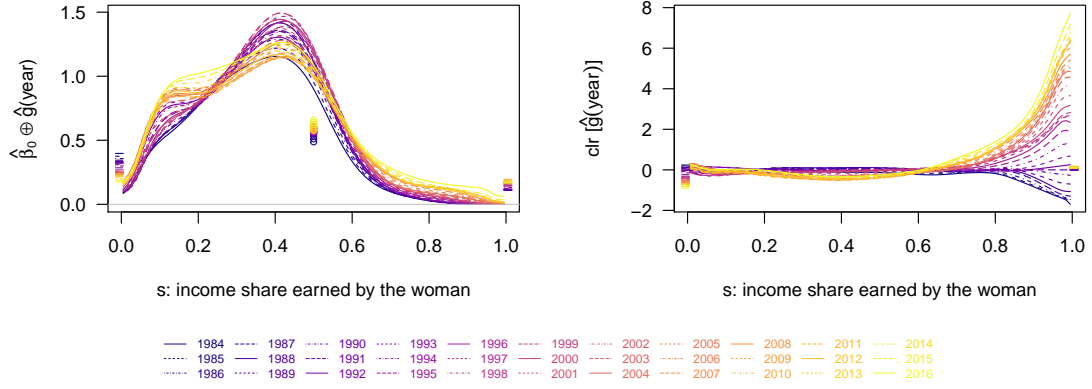


Figure E.13: Expected densities for couples without minor children living in *West* Germany over time [left] and clr transformed estimated effects of *year* [right].

Figure E.13 shows the flexible nonlinear effect of *year*. Here, we observe a clear temporal trend towards more dispersed distributions of shares in $(0, 1)$. In the left panel, this is clearly visible. The mode of the expected densities for couples without minor children living in *West* Germany stays approximately the same (about 0.4) with probability mass shifting outwards over time. In more recent years, the expected densities tend to have a second maximum further left and a heavier tail on the right. Furthermore, the expected relative frequency of non-working women ($s = 0$) decreases with time, while the frequency of single-earner women ($s = 1$) increases to now more similar levels. The clr transformed effects (right) support our finding of dispersing densities on $(0, 1)$. Before 1991, the clr transformed effects tend to be smaller for low and high income shares (e.g., for $t \in I_t = (0, 0.3) \cup (0.6, 1)$) than for income shares in between (e.g., for $s \in I_s = (0.35, 0.45)$). After 1991, this reverses. Thus, using (A.10), the odds of the probabilities for the outer region I_t versus the more central region I_s are smaller for earlier *years* than in later *years*. We can conclude that the probability of I_t increases and/or the probability of I_s decreases with time. The clr transformed effects get particularly large for high income shares $s < 1$, which is not visible on the level of the original densities, where the absolute values of the corresponding densities in this area are small (left). This is due to the multiplicative effect structure, for which small (absolute) differences can correspond to large relative differences within the densities.

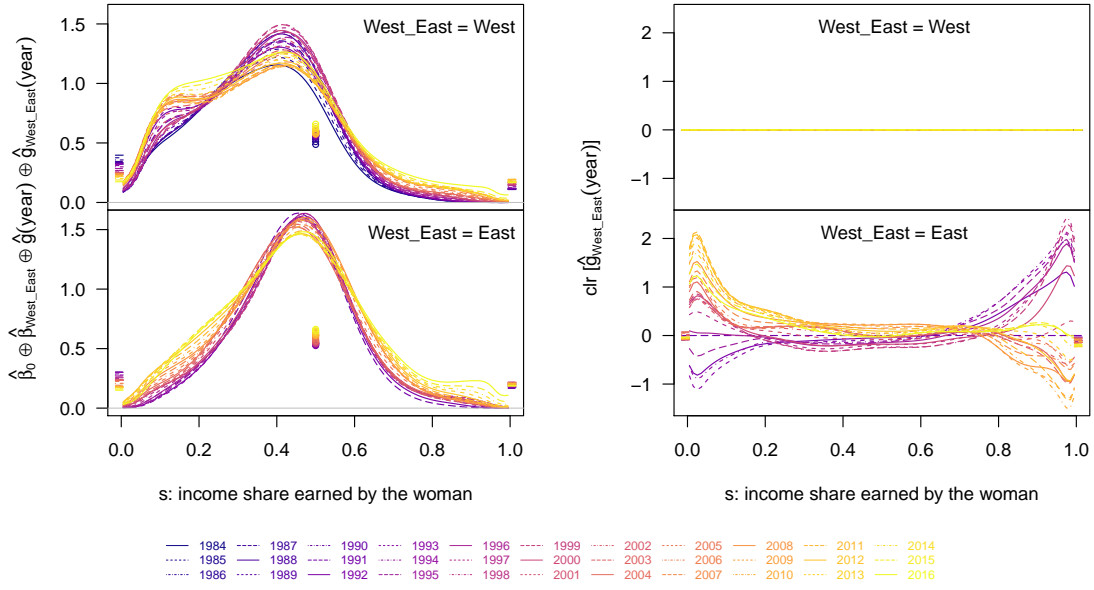


Figure E.14: Expected densities for couples without minor children living in *West* vs. *East* Germany over time [left] and clr transformed estimated interaction effects of *West_East* and *year* [right].

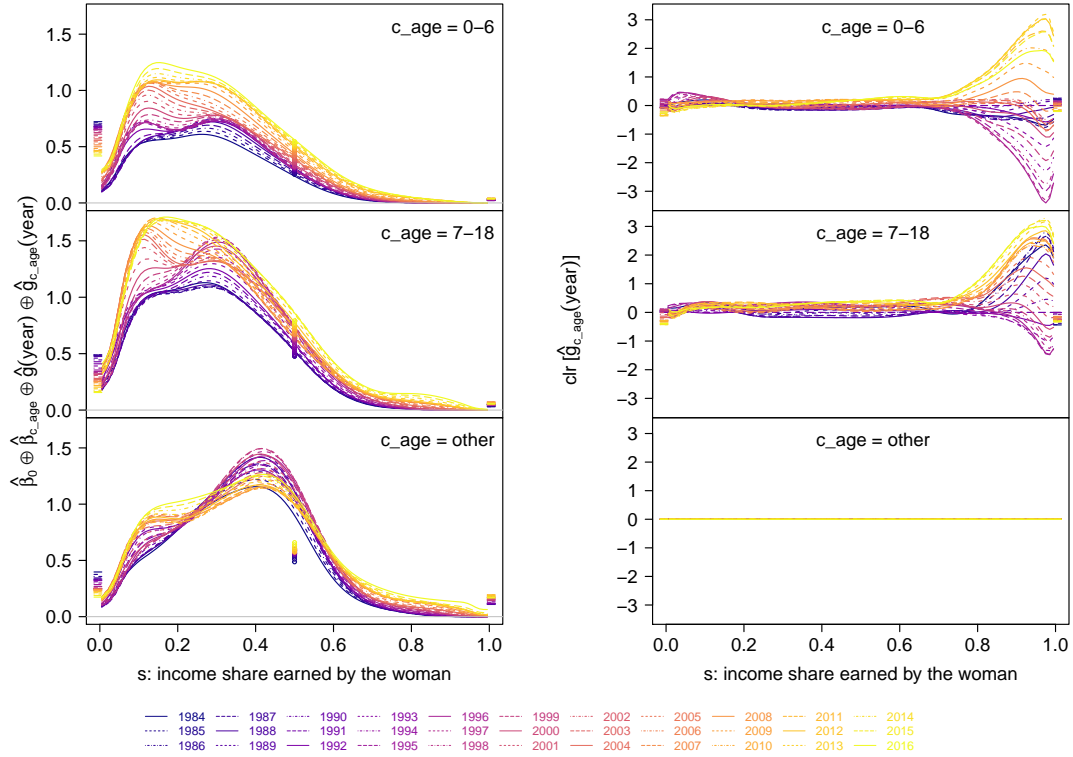


Figure E.15: Expected densities for couples living in *West* Germany for all three values of *c_age* over time [left] and clr transformed estimated interaction effects of *c_age* and *year* [right].

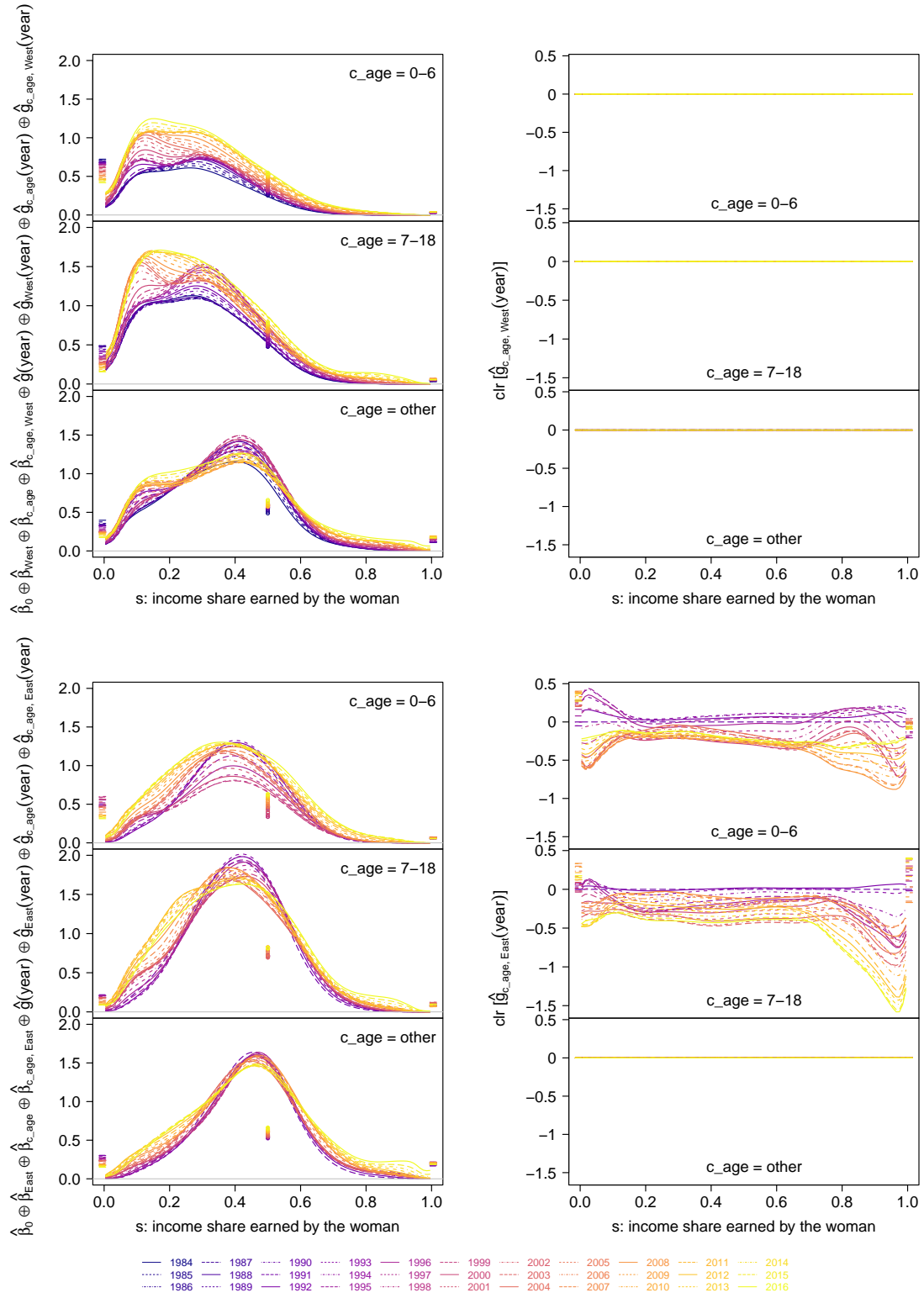


Figure E.16: Expected densities for couples living in *West* [top] vs. living in *East* Germany [bottom] for all three values of c_age over time [left] and clr transformed estimated interaction effects of c_age , $West_East$ and $year$ [right].

F Simulation study

F.1 Definition of relMSE

Consider the setting of our simulation study in Section 5. There, we use the relative mean squared error (relMSE) motivated by Brockhaus et al. (2015) to evaluate the goodness of the estimation results. For predictions and estimated partial effects it is defined as

$$\text{relMSE}(\hat{e}) := \frac{\frac{1}{v(\mathcal{Y})} \int_{\mathcal{Y}} \|E(y) \ominus \hat{e}(y)\|_{B^2(\mu)}^2 dv(y)}{\frac{1}{v(\mathcal{Y})} \int_{\mathcal{Y}} \|E(y) \ominus \bar{E}\|_{B^2(\mu)}^2 dv(y)} = \frac{\int_{\mathcal{Y}} \|E(y) \ominus \hat{e}(y)\|_{B^2(\mu)}^2 dv(y)}{\int_{\mathcal{Y}} \|E(y)\|_{B^2(\mu)}^2 dv(y)},$$

where \mathcal{Y} denotes the set $\{1, \dots, 552\}$ for predictions, the set of possible values for categorical covariates (group-specific effects), e.g., $\{West, East\}$ for the covariate *West_East*, or the observed range for scalar covariates (linear/flexible effects), e.g., [1984, 2016] for *year*. For effects depending on more than one covariate, \mathcal{Y} is the Cartesian product of the appropriate sets. The measure v is the counting measure, the Lebesgue measure, or a product measure thereof, respectively. The estimated densities are denoted by $\hat{e}(y) \in B^2(\mu)$ for $y \in \mathcal{Y}$, corresponding to $\hat{f}_i = \hat{f}(i), i \in \mathcal{Y}$ for predictions or $\hat{h}_j(\mathbf{x}), \mathbf{x} \in \mathcal{Y}$ for estimated effects. Analogously, the true densities are denoted by $E(y)$. Their overall mean, $\bar{E} := 1/v(\mathcal{Y}) \int_{\mathcal{Y}} \int_{\mathcal{T}} E(y) d\mu dv(y)$, is $0 \in B^2(\mu)$ as a constant.

F.2 RelMSEs and MSEs for all effects

Figure F.1 shows the complete simulation results. The left side illustrates the relMSEs (see Section 5) for the predictions and all partial effects. The boxplots on the right correspond to the respective mean squared errors (MSEs), i.e., the numerators of the relMSEs. Furthermore, the denominators, i.e., the mean squared norms of the true effects, are added in form of a blue “x”. The right side shows that larger relMSEs, in particular for $\hat{\beta}_{region}, \hat{\beta}_{c_age, West_East}, \hat{g}_{West_East}(year), \hat{g}_{c_age}(year)$, and $\hat{g}_{c_age, West_East}(year)$, arise from the mean squared norm of the true effects for the respective effects being small. This means, the relative mean squared errors are large, because the true effects are small but not because the errors are large.

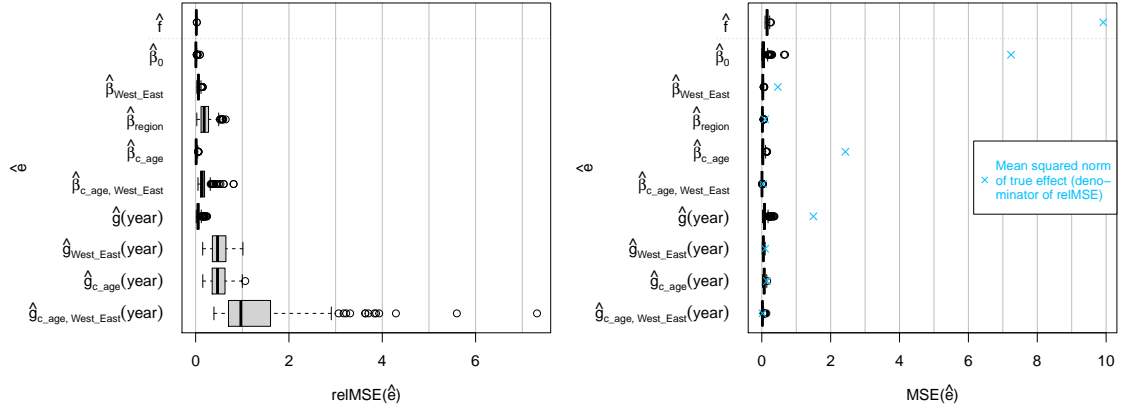


Figure F.1: RelMSE [left] and MSE [right] for predictions [top] and all partial effects [bottom].

F.3 Model selection

Table F.1 summarizes how many times effects are not selected over the 200 simulation runs. It contains the counts for the separately estimated continuous and discrete models, as well as for the final combined model in the last three columns, each of which sums up to 200 (total number of simulation runs). The rows of the table are grouped by the number of effects that are not selected in a simulation run, ranging from no effects (i.e., all effects are selected) to three effects. The table contains all effects (second column) that are not selected in at least one simulation run in either the continuous or the discrete model. These are exactly the four interaction effects. In particular, the main effects are selected in all simulation runs in both models (continuous and discrete). Note that as soon as one effect is selected in either the continuous or the discrete model, it is also selected in the combined model. Or, put differently, for an effect to be not selected in the combined model, it must not be selected in neither the continuous nor the discrete model. This explains that in the combined model, there are only few simulation runs, where an effect is not selected at all (4 in total), while for the separate models the numbers are noticeably higher. Most remarkably, in the continuous model, $\hat{\beta}_{c_age, West_East}$ is not selected in 131 simulation runs in total (including simulation runs, where additional effects are not selected).

	Effect(s) not selected	Number of simulation runs		
		continuous model	discrete model	combined model
All effects selected		60	163	196
One effect not selected	$\hat{\beta}_{c_age, West_East}$	118	0	0
	$\hat{g}_{West_East}(year)$	2	33	1
	$\hat{g}_{c_age}(year)$	2	1	1
	$\hat{g}_{c_age, West_East}(year)$	5	1	1
Two effects not selected	$\hat{\beta}_{c_age, West_East},$ $\hat{g}_{West_East}(year)$	1	0	0
	$\hat{\beta}_{c_age, West_East},$ $\hat{g}_{c_age}(year)$	3	0	0
	$\hat{\beta}_{c_age, West_East},$ $\hat{g}_{c_age, West_East}(year)$	8	0	0
	$\hat{g}_{West_East}(year),$ $\hat{g}_{c_age}(year)$	0	2	1
Three effects not selected	$\hat{\beta}_{c_age, West_East},$ $\hat{g}_{West_East}(year),$ $\hat{g}_{c_age}(year)$	1	0	0

Table F.1: Counts of effects not selected over the 200 simulation runs.

References

- Badiale, M. and Serra, E. (2011). *Semilinear Elliptic Equations for Beginners: Existence Results via the Variational Approach*. Springer Science & Business Media.
- Bertrand, M., Kamenica, E., and Pan, J. (2015). Gender Identity and Relative Income within Households. *The Quarterly Journal of Economics* **130**, 571–614.
- Boogaart, K. G. van den, Egozcue, J. J., and Pawlowsky-Glahn, V. (2010). Bayes linear spaces. *SORT: statistics and operations research transactions* **34**, 201–222.
- (2014). Bayes Hilbert Spaces. *Australian & New Zealand Journal of Statistics* **56**, 171–194.
- Brockhaus, S. and Rügamer, D. (2018). *FDboost: Boosting Functional Regression Models*. R package version 0.3-2.
- Brockhaus, S., Scheipl, F., Hothorn, T., and Greven, S. (2015). The functional linear array model. *Statistical Modelling* **15**, 279–300.
- Chen, S. X. (1999). Beta kernel estimators for density functions. *Computational Statistics & Data Analysis* **31**, 131–145.
- Egozcue, J. J., Díaz-Barrero, J. L., and Pawlowsky-Glahn, V. (2006). Hilbert Space of Probability Density Functions Based on Aitchison Geometry. *Acta Mathematica Sinica* **22**, 1175–1182.
- Elstrodt, J. (2011). *Maß- und Integrationstheorie*. Springer-Lehrbuch. Springer Berlin Heidelberg.

- Goebel, J., Grabka, M. M., Liebig, S., Kroh, M., Richter, D., Schröder, C., and Schupp, J. (2019). The German socio-economic panel (SOEP). *Jahrbücher für Nationalökonomie und Statistik* **239**, 345–360.
- Hothorn, T., Buehlmann, P., Kneib, T., Schmid, M., and Hofner, B. (2018). *mboost: Model-Based Boosting*. R package version 2.9-1.
- Jones, M. C. and Henderson, D. A. (2007). Miscellaneous Kernel-Type Density Estimation on the Unit Interval. *Biometrika* **94**, 977–984.
- Moss, J. and Tveten, M. (2018). *kdensity: Kernel Density Estimation with Parametric Starts and Asymmetric Kernels*. R package version 1.0.0.
- Petersen, A. and Müller, H.-G. (2016). Functional data analysis for density functions by transformation to a Hilbert space. *The Annals of Statistics* **44**, 183–218.
- Scott, D. W. (2015). *Multivariate Density Estimation: Theory, Practice, and Visualization*. 2nd ed. Hoboken, New Jersey: John Wiley & Sons, Inc.
- Wheeden, R. L. and Zygmund, A. (2015). *Measure and Integral: An Introduction to Real Analysis*. 2nd ed. CRC press.
- Wood, S. N. (2017). *Generalized Additive Models: An Introduction with R*. 2nd ed. Boca Raton: Chapman and Hall/CRC.